

Traffic4cast at NeurIPS 2021 – Temporal and Spatial Few-Shot Transfer Learning in Gridded Geo-Spatial Processes

<http://traffic4cast.ai> – <https://github.com/iarai/NeurIPS2021-traffic4cast>

Christian Eichenberger*	CHRISTIAN.EICHENBERGER@IARAI.AC.AT
Moritz Neun*	MORITZ.NEUN@IARAI.AC.AT
Henry Martin*†	HENRY.MARTIN@IARAI.AC.AT
Pedro Herruzo*	PEDRO.HERRUZO@IARAI.AC.AT
Markus Spanring*	MARKUS.SPANRING@IARAI.AC.AT
Yichao Lu†	YICHAO@LAYER6.AI
Sungbin Choi	SUNGBIN.CHOI.1@GMAIL.COM
Vsevolod Konyakhin§, Nina Lukashina¶,	
Aleksei Shpilman §	SEVAKONYAKHIN@GMAIL.COM
Nina Wiedemann†, Martin Raubal†	NWIEDEMANN@ETHZ.CH
Bo Wang**, Hai L. Vu**, Reza Mohajerpoor††, Chen Cai††,	
Inhi Kim††	BO.WANG1@MONASH.EDU
Luca Hermes§§, Andrew Melnik§§, Riza Velioglu§§,	
Markus Vieth§§, Malte Schilling§§	LUCAHERMES24@GMAIL.COM
Alabi Bojesomo ¶¶, Hasan Al Marzouqi¶¶,	
Panos Liatsis¶¶	ALABI.BOJESOMO@KU.AC.AE
Jay Santokhi***, Dylan Hillier***, Yiming Yang***, Joned Sarwar***,	
Anna Jordan***, Emil Hewage***	JAY@ALCHERATECHNOLOGIES.COM
David Jonietz †††	DAVID.JONIETZ@HERE.COM
Fei Tang †††	FEI.TANG@HERE.COM
Aleksandra Gruca†††	ALEKSANDRA.GRUCA@POLSL.PL
Michael Kopp*	MICHAEL.KOPP@IARAI.AC.AT
David Kreil*	DAVID.KREIL@IARAI.AC.AT
Sepp Hochreiter§§§*	SEPP.HOCHREITER@IARAI.AC.AT

Editor: tbd.

* Institute of Advanced Research in Artificial Intelligence (IARAI), Vienna, Austria

† Institute of Cartography and Geoinformation, ETH Zurich, Switzerland

‡ Layer 6 AI, Toronto, Canada

§ ITMO University, Saint Petersburg, Russia

¶ JetBrains Research, Saint Petersburg, Russia

|| HSE University, Saint Petersburg, Russia

** Institute of Transport Studies, Monash University, Clayton Victoria, Australia

†† CSIRO's Data61, Eveleigh, Australia

‡‡ Institute Civil and Environmental Engineering Department, Kongju National University, South Korea

§§ Machine Learning & Neuroinformatics Group, Bielefeld University, Germany

¶¶ Electrical Engineering and Computer Science Department, Khalifa University, Abu Dhabi, UAE

*** Alchera Data Technologies Ltd, Cambridge, UK

††† HERE Technologies, Zurich, Switzerland

††† Silesian University of Technology, Gliwice, Poland

§§§ Machine Learning Institute, Johannes Kepler University Linz, Austria

Abstract

The IARAI *Traffic4cast* competitions at NeurIPS 2019 and 2020 showed that neural networks can successfully predict future traffic conditions 1 hour into the future on simply aggregated GPS probe data in time and space bins. We thus reinterpreted the challenge of forecasting traffic conditions as a movie completion task. U-Nets proved to be the winning architecture, demonstrating an ability to extract relevant features in this complex real-world geo-spatial process. Building on the previous competitions, *Traffic4cast* 2021 now focuses on the question of model robustness and generalizability across time and space. Moving from one city to an entirely different city, or moving from pre-COVID times to times after COVID hit the world thus introduces a clear domain shift. We thus, for the first time, release data featuring such domain shifts. The competition now covers ten cities over 2 years, providing data compiled from over 10^{12} GPS probe data. Winning solutions captured traffic dynamics sufficiently well to even cope with these complex domain shifts. Surprisingly, this seemed to require only the previous 1h traffic dynamic history and static road graph as input.

1. Introduction

The global trends of urbanization and increased personal mobility force us to rethink the way we use urban space. The *Traffic4cast* competitions (Kreil et al., 2020; Kopp et al., 2021) tackle this problem in a data driven way, encouraging the application of the latest methods in machine learning to modeling complex spatial systems over time.

This year, we provide a unique data set derived from industrial scale trajectories of over 10^{12} raw GPS position fixes, with latitude, longitude, time stamp, as well as vehicle speed and driving direction recorded at that time. The data are made available by HERE Technologies and originate from a large fleet of vehicles. For the new temporal and spatial transfer learning challenges introduced in *Traffic4cast* 2021, we provide data for 10 culturally and socially diverse metropolitan areas around the world, covering a time span of 2 years.

The competition task was to predict from 1 hour traffic the next 5, 10, 15, 30, 45 and 60 min into the future. The training data was provided in the same format as last year (Kopp et al., 2021). An overview of the dynamic training data provided and the 1h test time slots to predict is shown in Figure 1. Along with each 1h test time slot, we provided the time of day and the day of the week but not the exact date. For each city, we provided a static graph derived from a road map in the same spatial resolution as the dynamic data, which could be used as mask or as a graph (Neun et al., 2021; Eichenberger and Neun, 2021).

For all cities considered, COVID-19 has lead to a visible shift in daily mobility traffic patterns, as can be seen by comparing traffic volumes from the pre-Covid (April/May 2019) and in-Covid data (April/May 2020), see also Neun et al. (2021) and Eichenberger and Neun (2021). Our **core challenge** requires participants to transfer learn across this domain shift (Ben-David et al., 2010; Wouter, 2018; Kouw and Loog, 2019; Webb et al., 2018; Gama et al., 2014; Widmer and Kubat, 1996) in traffic caused by the COVID-19 pandemic. This challenge is thus a **few-shot learning task** (Fei-Fei et al., 2006; Lu et al., 2020; Guo et al., 2019b), which requires to **transfer learn traffic dynamics across a temporal domain shift**.

Our **extended challenge** encourages participants to use all the data provided so far (data from 8 different cities for the pre-COVID era and 4 different cities during the in-COVID era) on two hitherto unseen cities for which no further training data is provided. For each city,

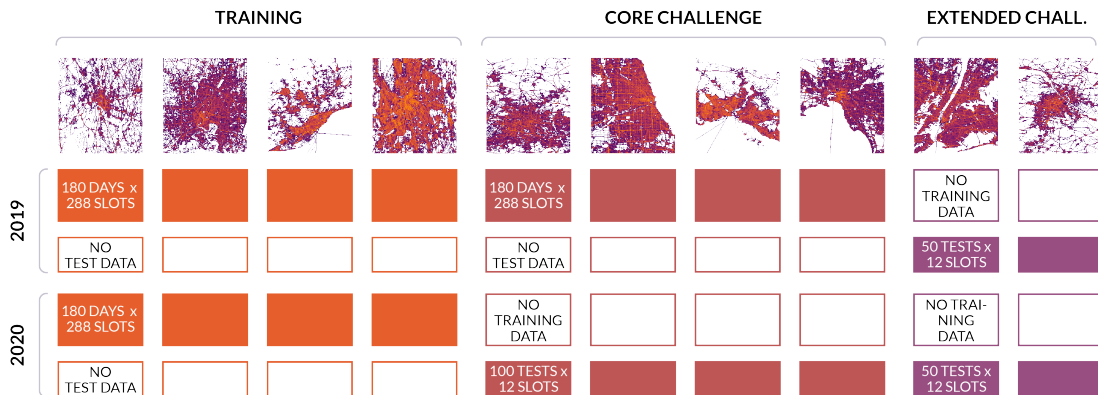


Figure 1: Data overview. There is data from 10 cities from 2019 and 2020. 4 cities are used for training (180 full days 2019 and 2020; 4 cities are used for the core challenge (180 full days 2019 pre-Covid and 100 test slots 2020 in-Covid); 2 cities are used for the extended challenge (50 test slots 2019 pre-Covid and 50 test slots 2020 in-Covid).

100 one-hour test time slots are randomly chosen, 50 from the pre-COVID era and 50 from the in-COVID era. The underlying machine learning challenge is thus a **few-shot transfer of traffic dynamics across a spatial and temporal domain shift**. It is noted that solutions to the extended challenge can be used as a solution for the core challenge as well, although participants will then make no use of the additional training data which might contain local, spatially relevant information. Apart from the static data and the test time slots, no further data from the target cities are exposed.

Informed by the previous *Traffic4cast* competitions (Kreil et al., 2020; Kopp et al., 2021), we chose two non-trivial baselines. For the core competition, we used a vanilla U-Net (Ronneberger et al., 2015) and trained models for each city separately for 4 epochs on the city’s 2019 training data only. For the extended competition, a Graph ResNet was used following Martin et al. (2020b). More details about the baselines can be found in Neun et al. (2021) and Eichenberger and Neun (2021).

The competition brings together a range of highly active fields in machine learning – few-shot learning, transfer learning, meta-learning more generally, as well as video frame prediction or graph based modelling. Compared to last year’s competition an order of magnitude more data was provided, covering ten cities across 2019 and 2020. This wealth of data was the basis for being able to tackle how far data and machine learning driven approaches alone can be used to decipher the implicit, largely unknown rules governing the phenomena of traffic by applying them across complex domain shifts.

The data encoding as Traffic Map Movies (Kreil et al., 2020), featuring multiple channels, provides a natural way to fuse information from multiple sources and show-cases the power of Machine Learning to excel at tasks that previously had to depend on domain knowledge, special data structures working on graphs (Snyder and Do, 2019), and manual feature engineering. Leading the way, this approach also proved itself in other domains such as rainfall prediction (Agrawal et al., 2019; Gruca et al., 2021; Herruzo et al., 2021), featured at CIKM and IEEE Big Data 2021 (<https://weather4cast.ai/>).

2. Standout Solutions

In the following, we give a short summary of outstanding solutions to our Traffic4cast 2021 competition. For each submission, we give a high-level diagram which we call inference diagram and which, in contrast to architecture diagrams typically used in the ML literature, summarizes the approach from an information-flow perspective, highlighting the trained models, the data used to train these models and to the ensembling of these trained models at inference time (if any). This sheds light on how the large and diverse amount of input data was used for the different tasks. The notation is the following: rectangles refer to data (test input, and test output); rounded rectangles represent functions in the inferences, arrows represent flow of information. We use square brackets to denote parameterized data or functions, bound to the parameters in the test input. For each model, after the colon, we also show the data the model was trained on, using the notation in Table 1, see ^d in caption.

2.1. oahciy: U-Net + Multi-Task Learning

Lu (2021) presents an amazingly simple multi-task learning framework by randomly sampling data from all available cities (4 training and 4 core) for all models in the ensemble. In the core competition 9 models were trained for 5 epochs while in the extended competition 7 models were trained for 50'000 steps only (8% of an epoch). The models are all U-Net with varying architecture and seeds. For more details see Table 1 and Appendix A.1.

Lu (2021) argues that this multi-task learning can be regarded as an implicit data augmentation and regularization technique when trained on one city only and forcing to learn city-agnostic representations thereby improving data efficiency. The implicit domain-adaptation through the addition of 2019 and 2020 data for at least one city is reported as crucial encouraging the model to learn to adapt to temporal domain shifts during training.

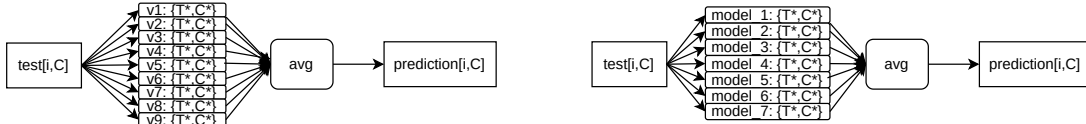


Figure 2: Inference oahciy (Lu, 2021) (left: core competition, right: extended competition).

2.2. sungbin: U-Net Ensemble

The approach of Choi (2021) is very similar to (Lu, 2021), also averaging ensembles of different U-Net architectures (4 city-independent models). In contrast to Lu (2021), Choi (2021) trained on target city training data, too (3 models in core). For more details see Table 1 and Appendix A.2.

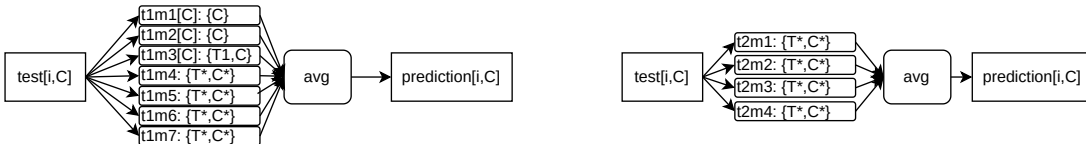


Figure 3: Inference sungbin (Choi, 2021) (left: core competition, right: extended competition).

2.3. sevakon: U-Net with Temporal Domain Adaptation

Konyakhin et al. (2021) also base their approach on the success of U-Nets in previous competitions. However, in contrast to (Lu, 2021) and (Choi, 2021), they train their models on each target city in the core competition only (they did not participate in the extended competition). They use three different architectures (vanilla U-Net, DenseNet, and EfficientNet (Tan and Le, 2019) pre-trained on Imagenet (Deng et al., 2009)), a static mask derived from dynamic data and a per-pixel and per-channel temporal domain-adaptation (TDA) factor. Their final prediction is derived from these 3 models; each model is used with and without TDA, resulting in 6 predictions to which the static mask is applied and which are then averaged.

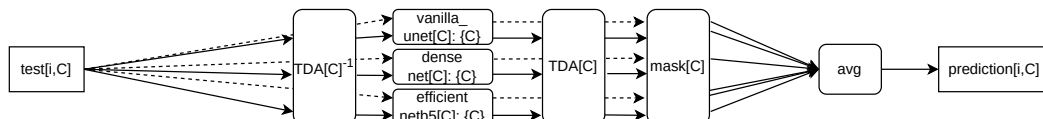


Figure 4: Inference sevakon (Konyakhin et al., 2021) (core competition). The city mask is derived from the training and test data.

2.4. nina: U-Net++ on Patches

Wiedemann and Raubal (2021) also use a U-Net variant, but in a patch-based manner, as it was shown to be beneficial in other segmentation tasks (Zhang et al., 2006; Ghimire et al., 2020) (also (Misra et al., 2020) in classification). No static road information was used. This method allowed them to use a parameter-heavier UNet++ with more skip connections (Zhou et al., 2019, 2018), which they suggest was helpful in light of the sparsity of the data. Patches are sampled from all available labelled data. After different experiments, choosing the available patches to be 100×100 crops with stride 10 was found to perform best. The patch-wise prediction exhibits an ensemble-like behavior.

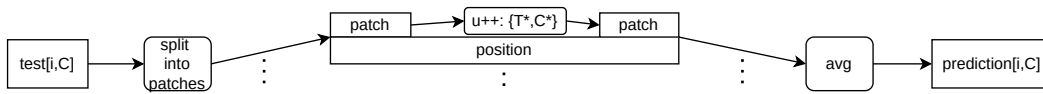


Figure 5: Inference nina (Wiedemann and Raubal, 2021) (core competition and extended competition).

2.5. ai4ex: SWIN-Transformer

Bojesomo et al. (2021) uses a Swin-UNet structure where all convolution blocks are replaced by shifted window self attention; downsampling in the encoder is achieved by trainable patch merging layers and upsampling by patch expanding layers in the decoder branch; skip connections are implemented by a combination of addition and concatenation.

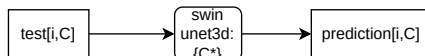


Figure 6: Inference ai4ex (Bojesomo et al., 2021) (core and extended competition).

2.6. dninja: Graph-Based U-Net

Hermes et al. (2022) present a graph based approach aiming at better generalization and transfer by leveraging knowledge of the underlying road network whilst ignoring areas without any traffic information. In order for their solution to make full use of the 2d topological information contained in the competition data they use 4 subgraphs corresponding to the provided 4 heading channels of said data.

2.7. resuly: 3DResNet and Sparse-UNet

Wang et al. (2021a) use a 3DResnet (Wang et al., 2021b) with 3D convolutions in 4 residual blocks and an output block. For the core competition, this output block consists of sequential CNN layers to restrain the temporal relationship. For the extended competition, the output block consists of a sparse U-Net (Graham, 2014; Choy et al., 2019) with data in Coordinate Format (COO) for the extended competition.

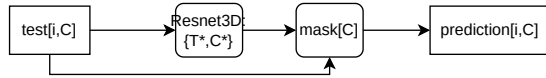


Figure 7: Inference resuly (Wang et al., 2021a) (left: core competition, right: extended competition). The mask is derived from the test data.

2.8. jaysantokhi: Dual-Encoding U-Net

Santokhi et al. (2021) use a dual encoding U-Net architecture aiming at a lightweight approach for real world deployments containing significantly fewer parameters (see also Table 1) and shorter training times. The architecture consists of two encoders one of which has skip connections to the decoder; encoder and decoder consist of Convolutional LSTM layers. The skip connections are not vanilla, but designed to carry the hidden and cell states of the encoder LSTM to the decoder LSTM, which is crucial for the approach. In both competitions, 4 models are pre-trained on the training cities and fine-tuned on the core competition cities. In the core competition, the city-specific fine-tuned model is used, whereas in the extended competition an architecture with fewer parameters is used and predictions are built by averaging over the outputs of all 4 models.

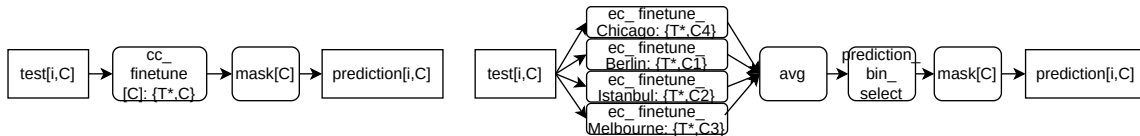


Figure 8: Inference jaysantokhi (Santokhi et al., 2021) (left: core competition, right: extended competition). The city mask is derived from test data.

3. Synopsis and Discussion

Looking at the different solutions above we see a large variety of mostly U-Net based approaches. Based on the experiences of the previous year (Kopp et al., 2021), this is not a complete surprise. However, it is interesting to see that for instance the simple averaging in ensembles in the winning solutions was also able to handle the domain shifts, even slightly outperforming some more tailored domain adaptation techniques. Table 1 highlights the key aspects and differences of the chosen architectures and informs the discussion below.

Team, rank (core/ext), approach	road graph, time-of-day, day-of-week ^a	models trained p. city ^b	#models trained ^c	Training datasets ^d	\sum #params core / ext ^e	mask ^f
oahciy (1/2) U-Net + multi-task learning (Lu, 2021)	road graph (concat)	no	9 / 7	$(9/7) \times \{T^*, C^*\}$	1710.2M / 17.1M	–
sungbin (2/1) U-Net Ensemble (Choi, 2021)	road graph (concat)	in two U-Nets	16/4	$2 \times \{C[1-4]\}; \{T1, C[1-4]\}; 4 \times \{T^*, C^*\} / 4 \times \{T^*, C^*\}$	123.6M / 33.9M	–
sevakon (3/-) U-Net with Temporal Domain Adaptation (Konyakhin et al., 2021)	no	yes	11/-	$3 \times \{C1\}; 2 \times \{C2\}; 3 \times \{C3\}; 3 \times \{C4\}$	342.0M / –	city (train/test data)
nina (6/3) U-Net++ on patches (Wiedemann and Raubal, 2021)	no	no	1=1	$\{T^*, C^*\}$	36.7M / 36.7M	–
ai4ex (4/6) SWIN-Transformer (Bojsomo et al., 2021)	no	no	1=1	$\{C^*\}$	141.9M / 141.9M	–
dninja (7/4) Graph-based U-Net (Hermes et al., 2022)	road graph, time-of-day, day-of-week	no	1=1	$\{T^*, C^*\}$	5.8M / 5.8M	by GNN
resuly (5/-) 3DResNet, Sparse-UNet (Wang et al., 2021a)	road graph	no	1/1	$\{T^*, C^*\}$	17.3M / 43k	test (test data)
jaysantokhi (8/5) Dual-Encoding U-Net (Santokhi et al., 2021)	no	after pre-training	4/4	$\{T^*, C[1-4]\}$	1.0M / 0.3M	city (test data)

Table 1: Synopsis. ^a what supplemental information is used; ^b whether some of the trained models used in the inference are specifically trained on the target city; ^c 9/7 means 9 models in the core and 7 different models in the extended competition, whereas 1=1 means the same trained model was used in both competition; ^d T1=Moscow, T2=Barcelona, T3=Antwerp, T4=Bangkok, C1=Berlin, C2=Istanbul, C3=Melbourne, C4=Chicago, E1=Vienna, E2=New York, T*=all training cities, C*=all core cities, E*=all extended cities. E.g. $(9/7) \times \{T^*, C^*\}$ means 9 models trained on all training and core competition cities for the core competition and 7 from the same cities for the extended competition, and $\{T^*, C[1-4]\}$ expands to a model for each city trained on all training cities plus one of the core cities; ^e Sum of trainable weights of all the model checkpoints used in the inference as extracted from the participants’ checkpoint using code in Eichenberger and Neun (2021); ^f Kind of mask used for post-processing.

3.1. Why were the same strategies successful in both competitions?

Lu (2021) won the core competition with an ensemble of models all trained with data from all training and core competition cities. This indicates that his solution already is able to capture spatial transfer, although at the price of a high amount of parameters (see Table 1). Hence, the combination of a diverse enough set of training cities with a large amount of data together with the static road information seems to be enough to solve both transfer learning challenges of our competition. Although the second placed approach of (Choi, 2021) is very similar, apart from minor architectural choices, the main difference is that Lu (2021) only has city-independent models. In contrast, the models by Konyakhin et al. (2021) trained only per city are competitive with regards to the temporal transfer. This again gives an indication that the explicit temporal domain-adaptation was necessary in this approach. In contrast, the first two ensembles (Lu et al., 2020; Choi, 2021) successfully did an implicit temporal adaptation through the city-independent models trained on data from multiple cities from before and after the temporal shift. Naively, we would have expected to see more domain-adaptation approaches in the core competition like the temporal domain-adaptations by (Konyakhin et al., 2021) or data augmentation techniques to use the test slot inputs for few-shot learning.

It is also remarkable to see that the patch-based approach of Wiedemann and Raubal (2021) is competitive especially for the spatial transfer in the extended challenge. The patches introduced an additional implicit level of ensemble learning within a city. This seems to have had a similar positive impact. The work of Bojesomo et al. (2021), Hermes et al. (2022) and Santokhi et al. (2021) show that transformers on patches, graph-based approaches and light-weight UNets are also able to handle the transfer tasks in both competitions with, in some cases, significantly smaller models (see Table 1).

In addition, we see clear traces of temporal averaging in the qualitative analysis of the outlier special prize (see Section 3.4 and Appendix C). Hence, it seems that non-distributional predictions evaluated by MSE seem to encourage trading off spatial, temporal, and channel-wise features jointly. A similar temporal and spatial “blurring” effect has been reported in weather forecasting (Ravuri et al., 2021b; Sønderby et al., 2020; Witt et al., 2021).

Finally, we can see that most approaches did not use any additional dynamic features such as time-of-day or day-of-week. Hence, 1h dynamic input data together with static data seems to capture the city-specific dynamics already, which models can and did then exploit in both our domain shift transfer learning challenges. Of course, one cannot exclude that completely different approaches than those considered and submitted by our competition participants could benefit from such additional features or that they could be beneficial in a different task setting (see Section 3.5).

3.2. Where do the submission performances differ?

We analyse the MSE loss for each solution above per directed cell (viewing all 4 headings of a pixel as virtual detector for volume and speed separately) – we bin these directional pixels by their standard deviation in the ground truth speed data (details and full analysis can be found in Appendix B). Thereby, we see where predictions are hard and where the competition was decided. We see that all models struggle in the same std ranges. Of course, MSE does not optimize each directed location independently, so the interpretation here

has to be taken *cum grano salis*. Referring to Figure 9, most of speed MSE losses for all

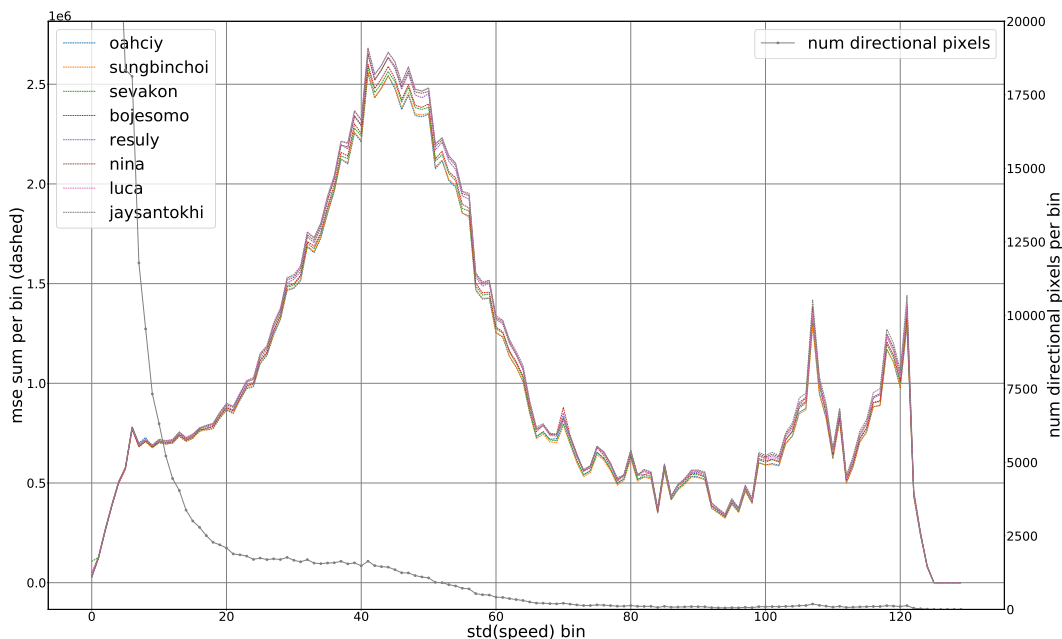


Figure 9: Relating MSE to std for speeds in BERLIN core: distribution of std among oriented pixels and summed MSE. The shaded gray areas highlights the two critical speed std ranges.

solutions under consideration come from the ranges 35–55 and 105–125 in speed std. If no data is collected, speed is set to 0, hence, the higher range implies an oscillation between very high speeds in the upper part of the value range $[0, 255]$ and no-data and all solutions seem to have struggled in providing accurate predictions. We localized these two ranges on the city map, see Appendix B, and observe: 35–55 speed std range tends to cover the main arteria and some long-range country roads with commuting traffic starting early in the morning; the 105–125 speed std range tends to cover areas with usually high speeds. This would hint at all solutions struggling where it is hard to find a good strategy of predicting speed in areas of very high variance and in the large area of medium standard deviation where the amount of such locations makes the total penalty so high.

3.3. What is the contribution of static road information?

Regarding static road information, Lu (2021) and Choi (2021) did not explicitly compare training with and without static road information as input. The patch-based approach of Wiedemann and Raubal (2021) does not use the static information; this might explain why this approach ranks lower in the core competition. We suppose that for many test inputs, the static road information is already in the dynamic data; however, in particular in areas of data sparsity, the static road information may be essential. So it remains unclear to what degree static information is required and, in particular, whether it helps in the critical ranges above.

3.4. What did models learn in outlier situations?

In order to tackle this questions, we asked participants to re-run their models on a new test set provided for our Outlier Special Prize. The test slots were from two cities of the core competition and the slots were quantitatively evaluated with a masked MSE. For the Special Prize, that mask only contained one pixel and two channels (hence $200 \cdot 6 \cdot 2$ integer values were evaluated against ground truth). These pixels were selected to contain a traffic jam situation reflected by a drastic drop in speed with a simultaneous increase in volume. In the examples analysed in Appendix C, the winning models of our core and extended competition predict a smoothed version of a jam resolution, underestimating speed and overestimating density. As MSE encourages model predictions to tend towards the mean in the data, they are never predicting a rare scenario such as a jam resolving more or less quickly than in expectation. In the selected outliers MSE for volume and speed is at the same level. More details on the heuristics and the design of our Outlier Special Prize can be found in Appendix C.

3.5. What did we learn about the metric?

Both challenges used the pixel-wise mean squared error (MSE) as a loss metric as it is also used in movie prediction tasks (Srivastava et al., 2015; Lee et al., 2018; Kwon and Park, 2019; Walker et al., 2016; Xue et al., 2016; Han et al., 2019; Oprea et al., 2020). From the analysis in previous subsections pertaining to this year’s competition challenges as well as from similar observations from our previous competitions (Kreil et al., 2020; Kopp et al., 2021), we are able to identify important, desirable properties a loss metric should have without currently being able to construct one. These properties are as follows.

Desired Property 1: The metric should not be distorted by missing values. Zero speed values in the case of no-data lead to a high variance in the speeds to predict in any temporally gridded bin. In contrast, zero volume for missing values does not affect the variance. A possible solution, suggested by Wiedemann and Raubal (2021), is to evaluate speed only in case of non-zero volume. With that models might be less defensive predicting speed.

Desired Property 2: The metric should be flexible in handling spatial and temporal shifts. Predicting just slightly at the wrong place leads to a double punishment, encouraging solutions that can be visually observed to show an ‘averaging phenomenon’ even in high scoring solutions as outlined in Qi and Kwok (2020). Shifts in traffic phenomena need to be handled depending on the application needs.

Desired Property 3: The metric should cope with different scales. Volume values can be heavily biased due to the fact that GPS probes are only collected by a fraction of the full traffic. Speed values are in most cases less biased (apart from idiosyncrasies such as (un)loading) but often cluster (e.g. around signaled speed limits under normal traffic conditions). In the competition no normalization was used on purpose, giving more weight to speed predictions. Furthermore, outlier situations are rare, but critical, and therefore tend to not be given enough weight compared to their utility by MSE. Hence, the metric should be able to incorporate multiple aggregation levels.

Desired Property 4: The metric should be distribution-aware. Single-value predictions tend to produce averaging scenarios as we see in the analysis of outliers (see Appendix C). Similar to Espeholt et al. (2021) and Ravuri et al. (2021a) predicting a possible distribution

instead of a single scalar could help estimating the uncertainty and evaluating at the distributional level. Such an approach would probably make most sense in combination with *Desired Property 2*.

3.6. Has transfer learning been achieved? In what sense?

If we think of the winning U-Net architecture (Lu, 2021), then models are able to combine global and local information to create a good average forecast. However, the pixel-wise MSE metric leads to models that do not yet cover sudden changes over time that can occur in real-world traffic dynamics (see Sections 3.4 and 3.5).

4. Summary and Outlook

It is encouraging to see that so many different machine learning approaches lead to competitive results in our map movie completion task. Winning solutions captured traffic dynamics sufficiently well to even cope with complex domain shifts. Surprisingly, this seemed to require only the previous 1h traffic dynamic history and static road graph as input. In addition, our competition results point to interesting future research directions and questions.

The pixel-wise MSE loss metric encouraged solutions that performed poorly on real-world relevant outlier situations with their prediction often being averaged scenarios. Improving on this metric may necessitate a range of relevant real-world tasks, each with their own external task-specific metric and reference data, such as predicting estimated times of arrival, ETA (Derrow-Pinion et al., 2021). In another domain, the climate extremes indices provide a standard catalogue of metrics (Alexander et al., 2021). The need to consider complementary domain specific tasks was recently also demonstrated in precipitation forecasting (Ravuri et al., 2021a; Espeholt et al., 2021). For traffic, unfortunately, there seems to be no such standard catalogue of application tasks, metrics, and data.

The *Traffic4cast* 2021 competition has proven again that representing traffic in a temporal and spatial grid is a powerful framework that allows for complex questions in traffic research to be addressed. The prediction of effects of road closures, changed speed limits, or an addition of lanes could thus be equally formulated in such a representation as simple completion tasks. Fundamental questions of classical traffic research can thus be approached in a purely data-centric, non-expert dependent way with the help of machine learning. Finally, it is of key interest to explore whether this framework can be adapted or extended to incorporate new data sources such as satellite data, loop counter data, or crowd-sourced traffic data. The necessary sensor fusion and cross-platform translation tasks are interesting applications of machine learning.

Acknowledgments

We would like to thank HERE technologies for making our competition data available.

References

- Shreya Agrawal, Luke Barrington, Carla Bromberg, John Burge, Cenk Gazen, and Jason Hickey. Machine learning for precipitation nowcasting from radar images. arXiv preprint arXiv:1912.12132, 2019. URL <https://arxiv.org/abs/1912.12132>.
- Lisa Alexander, Markus Donat, Margot Bador, Ian Macadam, Nicholas Herold, and Jonathan McComb. Climdex indices – the climdex indices can help us understand patterns in temperature and precipitation extremes: how they change from year to year or from place to place., 2021. URL <https://www.climdex.org/learn/indices/>. Accessed 2022-02-11.
- Luc Anselin. What is special about spatial data? alternative perspectives on spatial data analysis. Technical Report 89-4, National Center for Geographic Information and Analysis, University of California, Santa Barbara, 1989.
- S. Ben-David, J. Blitzer, K. Crammer, A. Kulesza, F. Pereira, and J. Vaughan. A theory of learning from different domains. Machine Learning, 79:151–175, 2010.
- Alabi Bojesomo, Hasan Al-Marzouqi, and Panos Liatsis. Swinunet3d – a hierarchical architecture for deep traffic prediction using shifted window transformers. arXiv preprint arXiv:2201.06390v1, 2021. URL <https://arxiv.org/abs/2201.06390v1>.
- Dominik Bucher, Francesca Mangili, Francesca Cellina, Claudio Bonesana, David Jonietz, and Martin Raubal. From location tracking to personalized eco-feedback: A framework for geographic information collection, processing and visualization to promote sustainable mobility behaviors. Travel behaviour and society, 14:43–56, 2019.
- Sungbin Choi. Traffic map prediction using unet based deep convolutional neural network. arXiv preprint arXiv:1912.05288, 2019. URL <https://arxiv.org/abs/1912.05288>.
- Sungbin Choi. Utilizing unet for the future traffic map prediction task traffic4cast challenge 2020. arXiv preprint arXiv:2012.00125, 2020. URL <https://arxiv.org/abs/2012.00125v1>.
- Sungbin Choi. Applying unet for the traffic map prediction across different time and space, 2021. URL <https://github.com/SungbinChoi/traffic4cast2021/blob/main/Paper.pdf>.
- Christopher Choy, JunYoung Gwak, and Silvio Savarese. 4d spatio-temporal convnets: Minkowski convolutional neural networks. In Proceedings of the IEEE Conference on Computer Vision and Pattern Recognition, pages 3075–3084, 2019.
- Jia Deng, Wei Dong, Richard Socher, Li-Jia Li, Kai Li, and Li Fei-Fei. Imagenet: A large-scale hierarchical image database. In 2009 IEEE Conference on Computer Vision and Pattern Recognition, pages 248–255, 2009. doi: 10.1109/CVPR.2009.5206848.
- Austin Derrow-Pinion, Jennifer She, David Wong, Oliver Lange, Todd Hester, Luis Perez, Marc Nunkesser, Seongjae Lee, Xueying Guo, Brett Wiltshire, and et al. Eta prediction with graph neural networks in google maps. Proceedings of the 30th ACM International

- Conference on Information & Knowledge Management, Oct 2021. doi: 10.1145/3459637.3481916. URL <http://dx.doi.org/10.1145/3459637.3481916>.
- Stephen Dunne and Bidisha Ghosh. Regime-based short-term multivariate traffic condition forecasting algorithm. Journal of Transportation Engineering, 138(4):455–466, 2011.
- Christian Eichenberger and Moritz Neun. Traffic4cast 2021 – temporal and spatial few-shot transfer learning in traffic map movie forecasting. <https://github.com/iarai/NeurIPS2021-traffic4cast>, July 2021. Accessed 2022-01-28.
- Alireza Ermagun and David Levinson. Spatio-temporal short-term traffic forecasting using the network weight matrix and systematic detrending. In Compendium of papers of Transportation Research Board 97th Annual Meeting, 2018a.
- Alireza Ermagun and David Levinson. Spatiotemporal traffic forecasting: review and proposed directions. Transport Reviews, 38(6):786–814, 2018b.
- Lasse Espeholt, Shreya Agrawal, Casper Sønderby, Manoj Kumar, Jonathan Heek, Carla Bromberg, Cenk Gazen, Jason Hickey, Aaron Bell, and Nal Kalchbrenner. Skillful twelve hour precipitation forecasts using large context neural networks. arXiv preprint arXiv:2111.07470, 2021. URL <https://arxiv.org/abs/2111.07470v1>.
- L. Fei-Fei, R. Fergus, and P. Perona. One-shot learning of object categories. IEEE transactions on pattern analysis and machine intelligence, 28(4):594–611, 2006.
- J. Gama, I. Zliobaite, A. Bifet, P. Mykola, and A. Bouchachia. A survey on concept drift adaptation. ACM Computing Surveys, 46(4), 2014. ISSN 0360-0300. doi: 10.1145/2523813.
- Kanchan Ghimire, Quan Chen, and Xue Feng. Patch-based 3d unet for head and neck tumor segmentation with an ensemble of conventional and dilated convolutions. In 3D Head and Neck Tumor Segmentation in PET/CT Challenge, pages 78–84. Springer, 2020.
- Google. COVID-19 Community Mobility Report. see how your community is moving around differently due to covid-19. <https://www.google.com/covid19/mobility?hl=en>. URL <https://www.google.com/covid19/mobility?hl=en>. Accessed 2021-03-30.
- Benjamin Graham. Spatially-sparse convolutional neural networks. arXiv preprint arXiv:1409.6070, 2014. URL <https://arxiv.org/abs/1409.6070>.
- Aleksandra Gruca, Pedro Herruzo, Pilar Ripodas, Andrzej Kucik, Christian Briese, Michael K. Kopp, Sepp Hochreiter, Pedram Ghamisi, and David P. Krel. CDCEO’21 - First Workshop on Complex Data Challenges in Earth Observation, page 4878–4879. Association for Computing Machinery, New York, NY, USA, 2021.
- Shengnan Guo, Youfang Lin, Ning Feng, Chao Song, and Huaiyu Wan. Attention based spatial-temporal graph convolutional networks for traffic flow forecasting. In Proceedings of the AAAI Conference on Artificial Intelligence, volume 33, pages 922–929, 2019a.
- Y. Guo, N. Codella, L. Karlinsky, J.R. Smith, T. Rosing, and R. Feris. A new benchmark for evaluation of cross-domain few-shot learning. arXiv preprint arXiv:1912.07200, 2019b. URL <https://arxiv.org/abs/1912.07200>.

- Tengda Han, Weidi Xie, and Andrew Zisserman. Video representation learning by dense predictive coding. In Proceedings of the IEEE International Conference on Computer Vision Workshops, pages 0–0, 2019.
- Luca Hermes, Andrew Melnik, Riza Velioglu, Markus Vieth, and Malte Schilling. A graph-based u-net model for predicting traffic in unseen cities. arXiv preprint arXiv:2202.06725, 2022. URL <https://arxiv.org/abs/2202.06725>.
- Pedro Herruzo and Josep L. Larriba-Pey. Recurrent autoencoder with skip connections and exogenous variables for traffic forecasting. In Hugo Jair Escalante and Raia Hadsel, editors, Proceedings of the NeurIPS 2019 Competition Track, volume 123 of Proceedings of Machine Learning Research, pages 0–0. PMLR, 2020.
- Pedro Herruzo, Aleksandra Gruca, Llorenç Lliso, Xavier Calbet, Pilar Rípodas, Sepp Hochreiter, Michael Kopp, and David P. Kreil. High-resolution multi-channel weather forecasting – First insights on transfer learning from the Weather4cast Competitions 2021. In 2021 IEEE International Conference on Big Data (Big Data), pages 5750–5757, December 2021. doi: 10.1109/BigData52589.2021.9672063.
- Amit Kumar Jaiswal, Ivan Panshin, Dimitrij Shulkin, Nagender Aneja, and Samuel Abramov. Semi-supervised learning for cancer detection of lymph node metastases. arXiv preprint arXiv:1906.09587, 2019. URL <https://arxiv.org/abs/1906.09587>.
- David Jonietz, Dominik Bucher, Henry Martin, and Martin Raubal. Identifying and interpreting clusters of persons with similar mobility behaviour change processes. In The Annual International Conference on Geographic Information Science, pages 291–307. Springer, 2018.
- Thomas N. Kipf and Max Welling. Semi-supervised classification with graph convolutional networks. arXiv preprint arXiv:1609.02907, 2017. URL <https://arxiv.org/abs/1609.02907v4>.
- Vsevolod Konyakhin, Nina Lukashina, and Aleksei Shpilman. Solving traffic4cast competition with u-net and temporal domain adaptation. arXiv preprint arXiv:2111.03421, 2021. URL <https://arxiv.org/abs/2111.03421>.
- Michael Kopp and David Kreil. Traffic4cast benchmarks and submission utilities for core competition. <https://github.com/iarai/NeurIPS2019-traffic4cast>, July 2019. Accessed 2021-02-17.
- Michael Kopp and David Kreil. Traffic4cast – our core competition 2020. <https://github.com/iarai/NeurIPS2020-traffic4cast>, July 2020. Accessed 2021-02-17.
- Michael Kopp, David Kreil, Moritz Neun, David Jonietz, Henry Martin, Pedro Herruzo, Aleksandra Gruca, Ali Soleymani, Fanyou Wu, Yang Liu, Jingwei Xu, Jianjin Zhang, Jay Santokhi, Alabi Bojesomo, Hasan Al Marzouqi, Panos Liatsis, Pak Hay Kwok, Qi Qi, and Sepp Hochreiter. Traffic4cast at neurips 2020 – yet more on the unreasonable effectiveness of gridded geo-spatial processes. In Hugo Jair Escalante and Katja Hofmann, editors, Proceedings of the NeurIPS 2020 Competition and Demonstration Track, volume

- 133 of Proceedings of Machine Learning Research, pages 325–343. PMLR, 2021. URL <http://proceedings.mlr.press/v133/kopp21a.html>.
- W. M. Kouw and M. Loog. A review of domain adaptation without target labels. IEEE transactions on pattern analysis and machine intelligence, October 2019. ISSN 0162-8828. doi: 10.1109/tpami.2019.2945942.
- David P Kreil, Michael K Kopp, David Jonietz, Moritz Neun, Aleksandra Gruca, Pedro Herruzo, Henry Martin, Ali Soleymani, and Sepp Hochreiter. The surprising efficiency of framing geo-spatial time series forecasting as a video prediction task – insights from the iara *Traffic4cast* competition at neurips 2019. In Hugo Jair Escalante and Raia Hadsell, editors, Proceedings of the NeurIPS 2019 Competition and Demonstration Track, volume 123 of Proceedings of Machine Learning Research, pages 232–241. PMLR, 08–14 Dec 2020. URL <http://proceedings.mlr.press/v123/kreil20a.html>.
- Yong-Hoon Kwon and Min-Gyu Park. Predicting future frames using retrospective cycle gan. In Proceedings of the IEEE Conference on Computer Vision and Pattern Recognition, pages 1811–1820, 2019.
- Ibai Lana, Javier Del Ser, Manuel Velez, and Eleni I. Vlahogianni. Road traffic forecasting: Recent advances and new challenges. IEEE Intelligent Transportation Systems Magazine, 10(2):93–109, 2018. doi: 10.1109/mits.2018.2806634.
- Alex X Lee, Richard Zhang, Frederik Ebert, Pieter Abbeel, Chelsea Finn, and Sergey Levine. Stochastic adversarial video prediction. arXiv preprint arXiv:1804.01523, 2018. URL <https://arxiv.org/abs/1804.01523>.
- Dong-Hyun Lee. Pseudo-label : The simple and efficient semi-supervised learning method for deep neural networks. ICML 2013 Workshop : Challenges in Representation Learning (WREPL), 07 2013.
- Aoyong Li, Pengxiang Zhao, He Haitao, Ali Mansourian, and Kay W. Axhausen. How did micro-mobility change in response to covid-19 pandemic? a case study based on spatial-temporal-semantic analytics. 2021. URL <https://www.research-collection.ethz.ch/handle/20.500.11850/473263>.
- J. Lu, P. Gong, J. Ye, and C. Zhang. Learning from very few samples: A survey, 2020.
- Yichao Lu. Learning to transfer for traffic forecasting via multi-task learning. arXiv preprint arXiv:2111.15542, 2021. URL <https://arxiv.org/abs/2111.15542>.
- Henry Martin, Ye Hong, Dominik Bucher, Christian Rupprecht, and René Buffat. *Traffic4cast*-traffic map movie forecasting–Team MIE-Lab. arXiv preprint arXiv:1910.13824, 2019. URL [url={https://arxiv.org/abs/1910.13824v2}](https://arxiv.org/abs/1910.13824v2).
- Henry Martin, Dominik Bucher, Ye Hong, René Buffat, Christian Rupprecht, and Martin Raubal. Graph-resnets for short-term traffic forecasts in almost unknown cities. In NeurIPS 2019 Competition and Demonstration Track, pages 153–163. PMLR, 2020a.

- Henry Martin, Dominik Bucher, Ye Hong, René Buffat, Christian Rupprecht, and Martin Raubal. Graph-ResNets for short-term traffic forecasts in almost unknown cities. In NeurIPS 2019 Competition and Demonstration Track, pages 153–163. PMLR, August 2020b. URL <http://proceedings.mlr.press/v123/martin20a.html>. ISSN: 2640-3498.
- Debaleena Misra, Carlos F Crispim-Junior, and Laure Tougne. Patch-based CNN evaluation for bark classification. In Workshop on Computer Vision Problems in Plant Phenotyping, Edinburgh, United Kingdom, August 2020. URL <https://hal.archives-ouvertes.fr/hal-02969811>.
- Moritz Neun, Christian Eichenberger, Michael Kopp, and David Kreil. Traffic4cast at neurips 2021 – competition design and data. arXiv preprint arXiv:TOBEPUBLISHED, 2021. URL <https://arxiv.org/abs/TOBEPUBLISHED>.
- Sergiu Oprea, Pablo Martinez-Gonzalez, Alberto Garcia-Garcia, John Alejandro Castro-Vargas, Sergio Orts-Escolano, Jose Garcia-Rodriguez, and Antonis Argyros. A review on deep learning techniques for video prediction. IEEE Transactions on Pattern Analysis and Machine Intelligence, 2020.
- Qi Qi and Pak Hay Kwok. Traffic4cast 2020–graph ensemble net and the importance of feature and loss function design for traffic prediction. arXiv preprint arXiv:2012.02115, 2020. URL <https://arxiv.org/abs/2012.02115>.
- Suman Ravuri, Karel Lenc, Matthew Willson, Dmitry Kangin, Remi Lam, Piotr Mirowski, Megan Fitzsimons, Maria Athanassiadou, Sheleem Kashem, Sam Madge, and et al. Skilful precipitation nowcasting using deep generative models of radar. Nature, 597(7878):672–677, Sep 2021a. ISSN 1476-4687. doi: 10.1038/s41586-021-03854-z. URL <http://dx.doi.org/10.1038/s41586-021-03854-z>.
- Suman Ravuri, Karel Lenc, Matthew Willson, Dmitry Kangin, Remi Lam, Piotr Mirowski, Megan Fitzsimons, Maria Athanassiadou, Sheleem Kashem, Sam Madge, Rachel Prudden, Amol Mandhane, Aidan Clark, Andrew Brock, Karen Simonyan, Raia Hadsell, Niall Robinson, Ellen Clancy, Alberto Arribas, and Shakir Mohamed. Skilful precipitation nowcasting using deep generative models of radar. Nature, 597(7878):672–677, September 2021b. ISSN 0028-0836, 1476-4687. doi: 10.1038/s41586-021-03854-z. URL <https://www.nature.com/articles/s41586-021-03854-z>.
- Olaf Ronneberger, Philipp Fischer, and Thomas Brox. U-net: Convolutional networks for biomedical image segmentation. In International Conference on Medical image computing and computer-assisted intervention, pages 234–241. Springer, 2015.
- Jay Santokhi, Dylan Hillier, Yiming Yang, Joned Sarwar, Anna Jordan, and Emil Hewage. Dual encoding u-net for spatio-temporal domain shift frame prediction. arXiv preprint arXiv:2110.11140, 2021. URL <https://arxiv.org/abs/2110.11140>.
- Corey Snyder and Minh Do. Streets: A novel camera network dataset for traffic flow. In H. Wallach, H. Larochelle, A. Beygelzimer, F. d'Alché-Buc, E. Fox, and R. Garnett, editors, Advances in Neural Information Processing Systems, volume 32. Cur-

- ran Associates, Inc., 2019. URL <https://proceedings.neurips.cc/paper/2019/file/ee389847678a3a9d1ce9e4ca69200d06-Paper.pdf>.
- Nitish Srivastava, Elman Mansimov, and Ruslan Salakhudinov. Unsupervised learning of video representations using lstms. In International conference on machine learning, pages 843–852, 2015.
- Strava. Strava releases 2020 year in sport data report. URL <https://blog.strava.com/press/yis2020/>. Accessed 2021-03-30.
- Casper Kaae Sønderby, Lasse Espeholt, Jonathan Heek, Mostafa Dehghani, Avital Oliver, Tim Salimans, Shreya Agrawal, Jason Hickey, and Nal Kalchbrenner. MetNet: A Neural Weather Model for Precipitation Forecasting. arXiv:2003.12140 [physics, stat], March 2020. URL <http://arxiv.org/abs/2003.12140>. arXiv: 2003.12140.
- Mingxing Tan and Quoc Le. Efficientnet: Rethinking model scaling for convolutional neural networks. In International Conference on Machine Learning, pages 6105–6114. PMLR, 2019.
- Jacob Walker, Carl Doersch, Abhinav Gupta, and Martial Hebert. An uncertain future: Forecasting from static images using variational autoencoders. In European Conference on Computer Vision, pages 835–851. Springer, 2016.
- Bo Wang, Reza Mohajerpoor, Chen Cai, Inhi Kim, and Hai L. Vu. Traffic4cast – large-scale traffic prediction using 3dresnet and sparse-unet. arXiv preprint arXiv:2111.05990, 2021a. URL <https://arxiv.org/abs/2111.05990>.
- Bo Wang, Hai L Vu, Inhi Kim, and Chen Cai. Short-term traffic flow prediction in bike-sharing networks. Journal of Intelligent Transportation Systems, pages 1–18, 2021b. ISSN 1547-2450.
- G.I. Webb, L.K. Lee, B. Goethals, and F. Petitjean. Analyzing concept drift and shift from sample data. Data Mining and Knowledge Discovery, 32:1179–1199, 2018.
- G. Widmer and M. Kubat. Learning in the presence of concept drift and hidden contexts. Machine learning, 23(1):69–101, 1996.
- Nina Wiedemann and Martin Raubal. Traffic forecasting on traffic moving snippets. arXiv preprint arXiv:2110.14383, 2021. URL <https://arxiv.org/abs/2110.14383>.
- Christian Schroeder de Witt, Catherine Tong, Valentina Zantedeschi, Daniele De Martini, Alfredo Kalaitzis, Matthew Chantry, Duncan Watson-Parris, and Piotr Bilinski. RainBench: Towards Data-Driven Global Precipitation Forecasting from Satellite Imagery. Proceedings of the AAAI Conference on Artificial Intelligence, 35(17):14902–14910, May 2021. ISSN 2374-3468. URL <https://ojs.aaai.org/index.php/AAAI/article/view/17749>. Number: 17.
- M. K. Wouter. An introduction to domain adaptation and transfer learning. arXiv preprint arXiv:1812.11806, abs/1812.11806, 2018. URL <https://arxiv.org/abs/1812.11806>.

- Fanyou Wu, Yang Liu, Zhiyuan Liu, Xiaobo Qu, Rado Gazo, and Eva Haviarova. Tlab: Traffic map movie forecasting based on hr-net. arXiv e-prints, pages arXiv–2011, 2020.
- Tianfan Xue, Jiajun Wu, Katherine Bouman, and Bill Freeman. Visual dynamics: Probabilistic future frame synthesis via cross convolutional networks. In Advances in Neural Information Processing Systems, pages 91–99, 2016.
- Wei Yu, Yichao Lu, Steve Easterbrook, and Sanja Fidler. Crevnet: Conditionally reversible video prediction. arXiv preprint arXiv:1910.11577, 2019.
- Lei Zhang, Xun Wang, Nicholas Penwarden, and Qiang Ji. An image segmentation framework based on patch segmentation fusion. In 18th International Conference on Pattern Recognition (ICPR’06), volume 2, pages 187–190. Ieee, 2006.
- Zongwei Zhou, Md Mahfuzur Rahman Siddiquee, Nima Tajbakhsh, and Jianming Liang. Unet++: A nested u-net architecture for medical image segmentation. In Deep learning in medical image analysis and multimodal learning for clinical decision support, pages 3–11. Springer, 2018.
- Zongwei Zhou, Md Mahfuzur Rahman Siddiquee, Nima Tajbakhsh, and Jianming Liang. Unet++: Redesigning skip connections to exploit multiscale features in image segmentation. IEEE Transactions on Medical Imaging, 2019.

Appendices

Appendix A. Standout Solution Details

This appendix gives more details on the leaderboard contributions. In the section header, we give the paper title along with their achieved ranks in the core/extended competition in parentheses. For each submission, we also give an inference diagram which in our opinion is supposed to summarize the approach from an information-flow perspective by linking to the trained models, the data used in training rather than to the architecture details and to the ensembling.

A.1. oahciy: U-Net + Multi-Task Learning

(Lu, 2021) presents an amazingly simple multi-task learning framework by randomly sampling data from all available cities and training the models to jointly predict future traffic for different cities. (Lu, 2021) uses ensembles by averaging 9/7 different U-Net models with varying architecture and seeds, all trained on all data for 4 training cities and 4 core cities. The models in the core competition are trained for 5 epochs, the models for the extended competition for 50'000 steps only.

(Lu, 2021) argues that the multi-task learning can be regarded as an implicit data augmentation and regularization technique preventing overfitting when trained on one city only and forcing to learn city-agnostic representations and improving data efficiency. (Lu, 2021) reports the results of a comparison with a series of domain-adaptation techniques and find that their approach is superior in both competitions and report to have tried different ensembling techniques. For temporal domain adaptation, he conducted experiments by using 3 of the training cities as training data and 1 city (Bangkok) for evaluation; his findings suggest that training on the target city is crucial in comparison to more data from the 3 training cities and that adding 2019 and 2020 data for at least one city is crucial encouraging the model to learn to adapt to temporal domain shifts during training. With respect to the core competition, they achieved good performance in the extended competition by reducing the number of parameters in the U-Net model and adopting an early stopping strategy. (Lu, 2021) suggests performance could be improved by fine-tuning models in a city-dependent manner and using manually designed features like time of day.

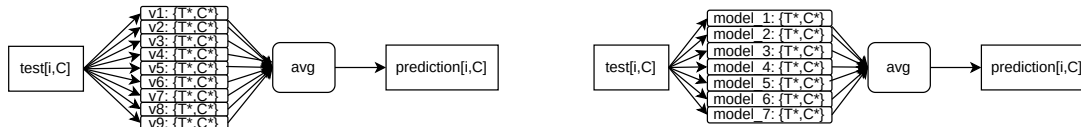


Figure 10: Inference oahciy (Lu, 2021) (left: core competition, right: extended competition).

A.2. sungbin: U-Net Ensemble

The approach of (Choi, 2021) is very similar to (Lu, 2021), also using different U-Net architectures and averaging ensembles. In contrast to (Lu, 2021), (Choi, 2021) trains on target city-dependent training data, too, resulting in ensembles of 16/4 models in the two

competitions; each prediction comes from an ensemble of 7/4 models, of which 3/- are city-dependent. (Choi, 2021) reports that in previous participations (Choi, 2019, 2020) having training data from different cities hurt performance; (Choi, 2021) suggests that the additional cities for training only make the difference; however, no ablation studies are presented for this claim. As Berlin and Istanbul are in the core competition target cities as in the previous competition, we miss the exploration of the performance of last year’s approach and of the contribution of static road data.

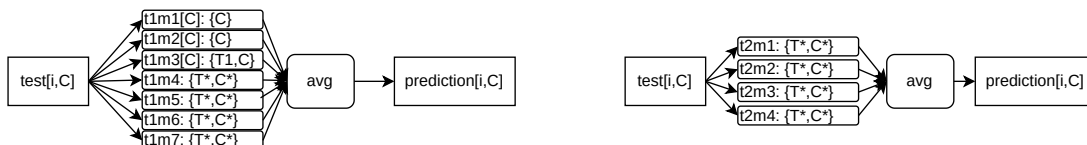


Figure 11: Inference sungbin (Choi, 2021) (left: core competition, right: extended competition).

A.3. sevakon: U-Net with Temporal Domain Adaptation

(Konyakhin et al., 2021) also base their approach on the success of U-Nets in previous competitions. However, in contrast to (Lu, 2021) and (Choi, 2021), they train their models on the target city in the core competition only (they did not participate in the extended competition). They use three different architectures (vanilla U-Net, DenseNet, and EfficientNet pre-trained on Imagenet (Deng et al., 2009)), a static mask derived from dynamic data and a per-pixel and per-channel temporal domain-adaptation factor. Their final prediction is derived from the 3 models; each model is used with and without TDA, resulting in 6 predictions to which the static mask is applied and which are then averaged. They find slightly better results are achieved by using a static pixel-wise binary mask generated from the training and test data for non-zero values among all channels. In addition to their TDA heuristics, (Konyakhin et al., 2021) also investigated pseudo-labelling without improvement; pseudo-labels are generated by applying the model on the (unlabelled) samples from the target domain and use these in training; pseudo-labelling had been used as an entropy regularization for probabilistic multi-class classification tasks (Jaiswal et al., 2019; Lee, 2013).

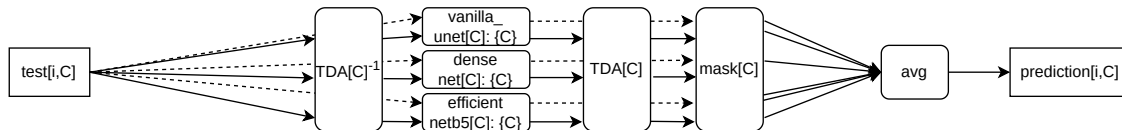


Figure 12: Inference sevakon (Konyakhin et al., 2021) (core competition). The city mask is derived from the training and test data.

A.4. nina: U-Net++ on Patches

(Wiedemann and Raubal, 2021) also use a U-Net variant, but in patch-based manner, as it was shown beneficial in other segmentation tasks (Zhang et al., 2006; Ghimire et al., 2020)

(also (Misra et al., 2020) in classification), without using the static road information. Using patches allowed them to use parameter-heavier UNet++ with more skip connections (Zhou et al., 2019, 2018), which they suggest to have been helpful in light of the sparsity of the data. They subsample from the available labelled data, processing 1000 patches for two epochs and then re-sampling (10 patches from 100 files). At inference time, the predictions are built by averaging the per-cell predictions from all patches that contain the cell.

They compare different model variants and different patch sizes and strides; their best performance was achieved in both competitions with quadratic 100×100 patches and stride 10. They show that the ensemble-like behaviour of patch-wise prediction accounts for small but significant increase in performance with smaller strides; they argue that the main advantage of the method lies in the simplification of the problem by splitting the data into smaller parts. Furthermore, (Wiedemann and Raubal, 2021) did an error analysis: the overwhelming part of the error is due to the predictions in the speed channels and volumes are zero most of the time. They further looked into those cells with non-zero volume data and derive speed MSE on those cells, which seems to be “hardly better than chance”, at least for a small validation set from the labelled data. They even investigated into training with a loss function that masked out speed on zero ground truth volumes. At test time, the speed of zero-predicted-volumes is imputed with zero. However, the current competition metric does not reflect the joint volume-speed distribution directly and under MSE different speed predictions might be less penalized. In discussion, the authors also pointed out that MSE masked this way might incentivize models to learn to predict “free flow speed” (*i. e.* speeds taken without the presence of other vehicles, see *e. g.* https://en.wikipedia.org/wiki/Fundamental_diagram_of_traffic_flow) in case of zero volume or a speed appropriate to the current traffic situation and not needing to gamble for the data collection gaps (as the GPS probes come from vehicle fleets representing only a part of total traffic).

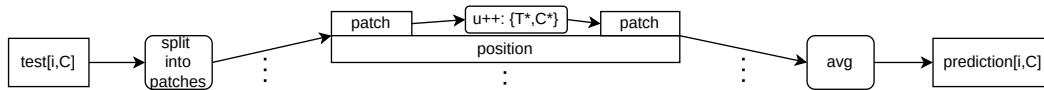


Figure 13: Inference nina (Wiedemann and Raubal, 2021) (core competition and extended competition).

A.5. ai4ex: SWIN-Transformer

(Bojesomo et al., 2021) uses a Swin-UNet structure where all convolution blocks are replaced by shifted window self attention; downsampling in the encoder is achieved by trainable patch merging layers and upsampling by patch expanding layers in the decoder branch; skip connections are implemented by a combination of addition and concatenation. The paper compares 3 different configurations with different embedding dimensions, feature mixing to find the best model in the leaderboard.

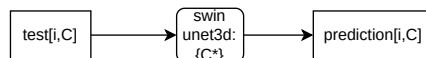


Figure 14: Inference ai4ex (Bojesomo et al., 2021) (core and extended competition).

A.6. dninja: Graph-Based U-Net

(Hermes et al., 2022) are the only graph-based contribution in the competition; they aim to leverage prior knowledge on the underlying structure of the street network, ignoring areas without any traffic information, and thereby to achieve better generalization and transfer by using a graph-based approach. Vanilla graph layers do not capture 2-dimensional topology like CNNs do – in order to capture this information, they enhance existing graph layers by using 4 subgraphs corresponding to the 4 headings of the challenge data. They show that these subgraphs are consistently beneficial for all cities; edge features contain a CNN-based embedding of the road graph as image; a global state vector contains the summed-up and scaled node features and encoding of time of day and day of week. (Hermes et al., 2022) use these Graph layers in a UNet architecture, where the 2D node positions are used for up and downsampling on graphs: downsampling works by taking the feature-wise max of node and edge features, while upsampling works by introducing edges from the input graph to the target graph and using graph propagation. This up- and downsampling approach effectively expands the receptive field of the graph approach without requiring too deep GNNs, which are thought to lead performance drop at a certain depth. Although ablation studies and extensive hyperparameter tuning are missing in their work, the work seems promising.

A.7. resuly: 3DResNet and Sparse-UNet

(Wang et al., 2021a) use 3DResnet (Wang et al., 2021b) with 3D convolutions in 4 residual block and an output block of sequential CNN layers to restrain the temporal relationship in the core competition and Sparse U-Net (Graham, 2014; Choy et al., 2019) with data in Coordinate Format (COO) for the extended competition. They enhance data loading by two-level shuffling over day files and then over indices, randomly picking up a number of files as training samples in each epoch. To ensure spatial and temporal diversity, these day files need to include all available cities in 2019 and 2020 and cover all seven days of the week. They show large training speed-ups for the Sparse UNets. Comparing the two approaches by training on each city separately, they find no consistently better method, with considerable differences in the convergence behaviour and the final loss achieved; above all, they conjecture that sparse UNets generalize better on the extended challenge but perform worse on the core challenge, however without giving systematic comparison of the same method applied in both settings.

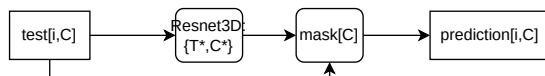


Figure 15: Inference resuly (Wang et al., 2021a) (left: core competition, right: extended competition). The mask is derived from the test data.

A.8. jaysantokhi: Dual-Encoding U-Net

(Santokhi et al., 2021) use a dual encoding U-Net architecture aiming at a lightweight approach for real world deployments containing significantly fewer parameters and shorter training times. The architecture consists of two encoders one of which has skip connections

to the decoder; encoder and decoder consist of Convolutional LSTM layers. The skip connections are not vanilla, but designed to carry the hidden and cell states of the encoder LSTM to the decoder LSTM, which is crucial for the approach. In both competitions, 4 models are pre-trained on the training cities and fine-tuned on the core competition cities. In the core competition, the city-specific fine-tuned model is used, whereas in the extended competition an architecture with fewer parameters is used and predictions are built by averaging over the outputs of all 4 models; in addition, in the core competition, the model outputs directly 6 frames, whereas the model in the extended competition outputs 12 frames. In both competition, a mask derived from the test data was found to be more performant than the static mask or mask based on the training data.

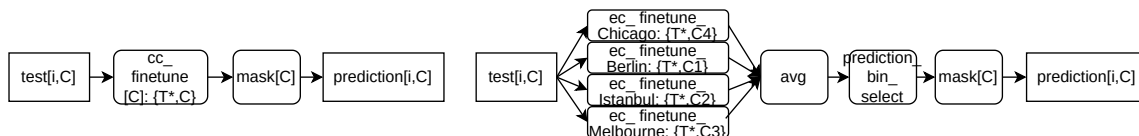


Figure 16: Inference jaysantokhi (Santokhi et al., 2021) (left: core competition, right: extended competition). The city mask is derived from test data.

Appendix B. Relating MSE to the Variance in the Data: Where do Models Struggle?

Here, we detail on Section 3.2.

For the analysis, we took standard deviation on the ground truth data of the 100 tests of the core competition (*i. e.* 18 time bins each, the 1 hour input and the 6 prediction slots from the 1 hour prediction horizon, see (Neun et al., 2021) for the test slot sampling details). We compute MSE for each directional pixel ($863280 = 495 \cdot 436 \cdot 4$ in total), separately for volume and speed. Finally, we plot MSE per std bin to find “hot spots”.

B.1. Relating speed variance to speed MSE

We have a strong asymmetry in the MSE levels in both competitions (see Figure 32), *e. g.* for Lu (2021), the winner of our core competition, we have `speed_mse: 148.427`, `vol_mse: 10.440`, `all_mse: 79.434` for MSE on the city of Berlin only (plots and data can be found in Eichenberger and Neun (2021)). Therefore, we put the focus of our analysis on relating speed variance to speed MSE. If we bin the test data by speed standard deviation as in Figure 17, we see that most directional pixels have little standard deviation. This is indicated by the gray line going down almost monotonically showing the counts for every speed std bin. Also notice that we do not show the full y range on the left.

If we relate this to MSE for speed of the submissions in the core competition, we see that speed MSE per directional pixel in the bin is going up almost monotonically and faster than in a linear fashion Figure 17. The curves of the different participants are pretty in parallel, so it looks as if they struggle at the same places. The different participants are represented by different colors.

If we multiply the two curves of Figure 17 top, we get the dashed curves of Figure 17 bottom, which shows the sum of the MSEs of all directional pixels in the bin. This allows us to see which speed std areas contribute most to the total speed MSE. The monotonic growing solid curve are the cumulative sums of the dashed ones, containing the same information as the dashed ones. A peak in the dashed curves is reflected by steepness in the solid curve. The final value top right is the sum over all (495, 436, 4) virtual speed detectors of the city, summing the per-pixel and per-heading MSE over all 100 test slots. If we divide the final cumulated number by the the number of such directional pixels, we get the `speed_mse` of 148.

We find two critical ranges of speed std where most of the final MSE is accumulated: around 35–55 and around 105–125. In the lower critical range (35–55), average MSE per speed std bin more than, doubles and increases monotonically, while the number of pixels per bin is slightly decreasing, which cumulates heavily; so despite the medium average MSE level, this translates into a peak in the per-bin cumulated MSE bin curves. The higher band (105–125) covers very high average MSE, but at a low number of pixels, which also translates into a peak.

B.1.1. MAPPING OUT THE TWO CRITICAL RANGES

We now visualize the locations of these two critical speed std ranges.

Figure 18 shows the locations of the 35–55 speed std band on the left side. This covers the main arteria as well as parts of long-range country roads where commuting traffic starts

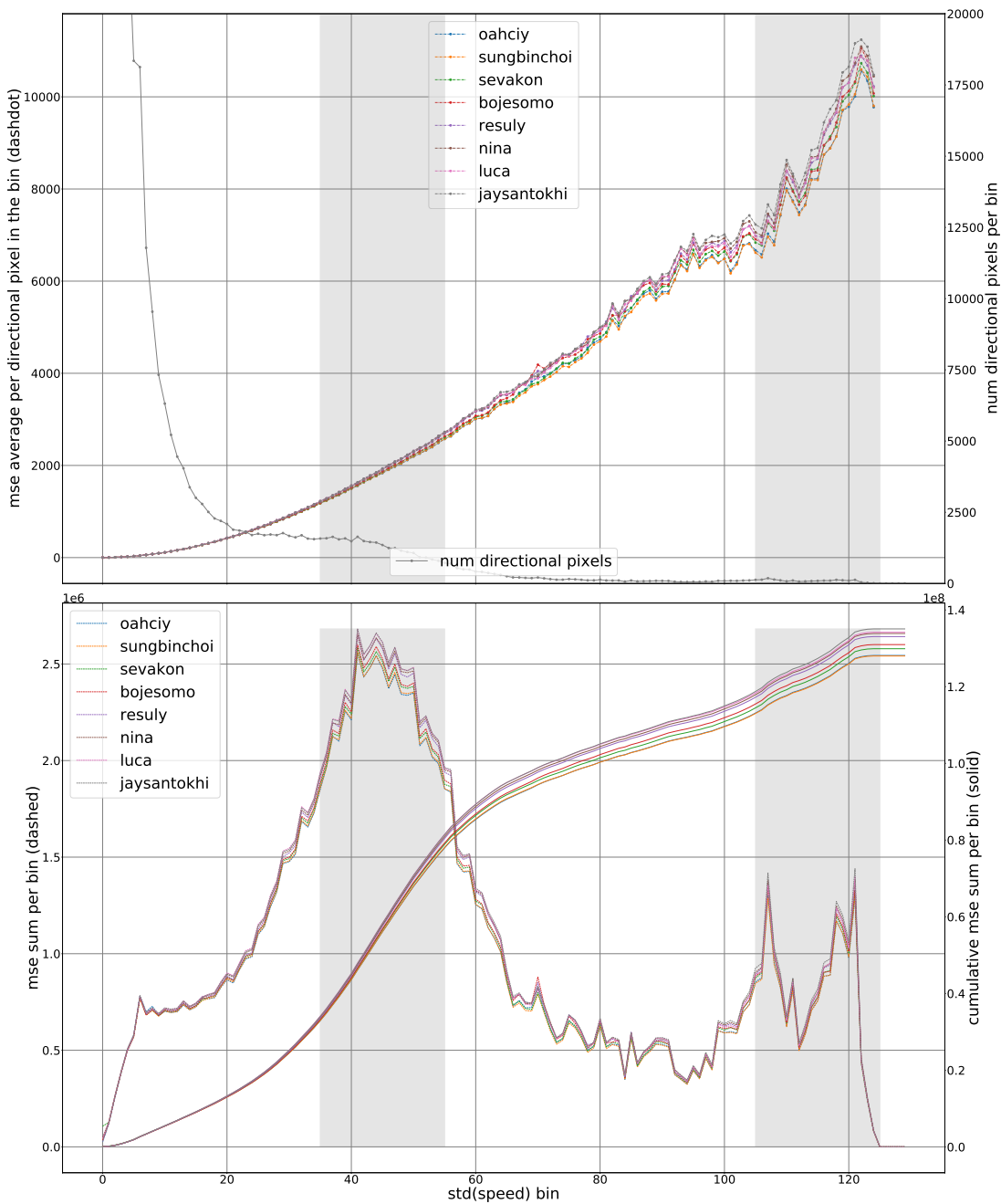


Figure 17: Relating MSE to std for speeds in BERLIN core: distribution of std among directional pixels (axis capped) and average MSE (top); summed MSE and cumulated summed MSE (bottom).

early in the morning. So these may be areas that are naturally hard to predict. This stems on the one hand from medium “free flow speeds” and high speed variance or no data, and on the other hand from relatively high “free flow speeds” and a lot of no-data in off-peak times.

The 105–125 speed std band on the right side in Figure 18 shows areas with usually high speeds and some no-data during the night.

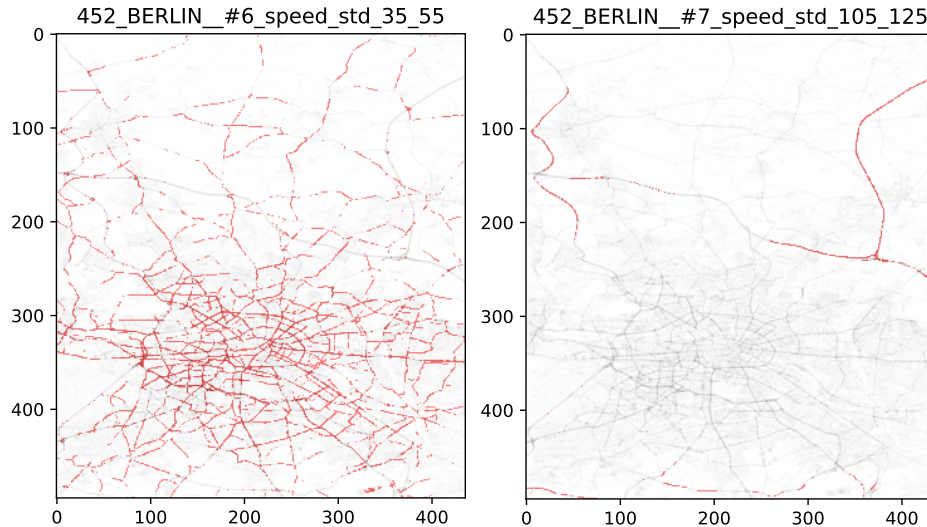


Figure 18: Locations (red) of the 35–55 (left) and 105–125 (right) speed std bands

B.1.2. REVISITING 3 BERLIN LOCATIONS

If we take each cell and heading as a speed detector, we have $495 \cdot 436 \cdot 4$ virtual speed detectors. We can now plot the mean against the std speed for data collected from the test slots of the core competition, see Figure 19. Each dot corresponds to one cell in the grid

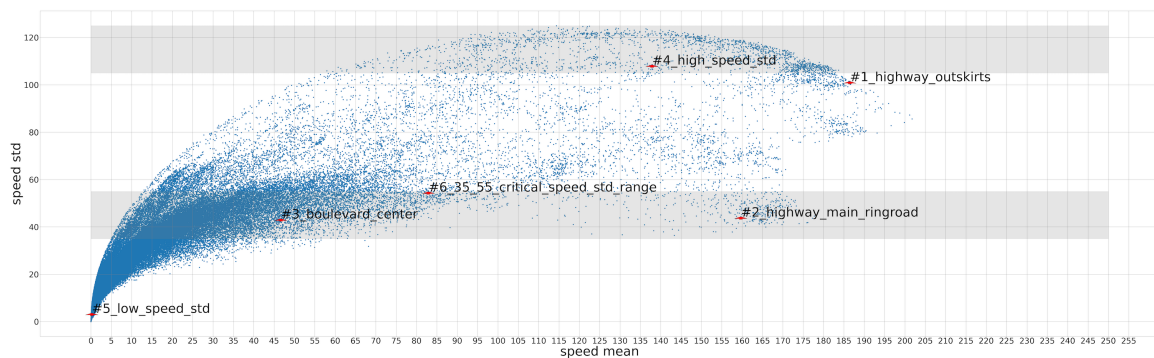


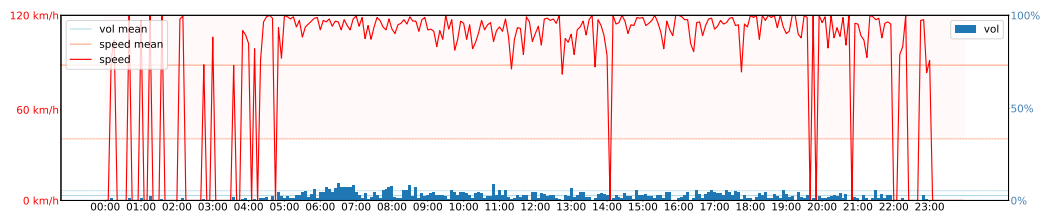
Figure 19: Critical ranges and sample situations in Berlin.

and one heading. Since a lot of cells never encounter any GPS probes, most of those points are close to the origin of the mean-std coordinates system. We choose 6 Berlin locations in Figure 20. In Figure 21, we plot volumes and speeds for one sample day for each of them and discuss these illustration with respect to the two critical ranges.

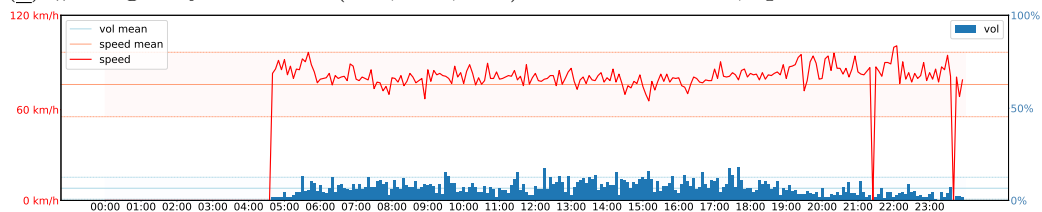


Figure 20: Speed std heatmap for Berlin showing the max of all 4 headings per pixel, showing the 3 Berlin locations.

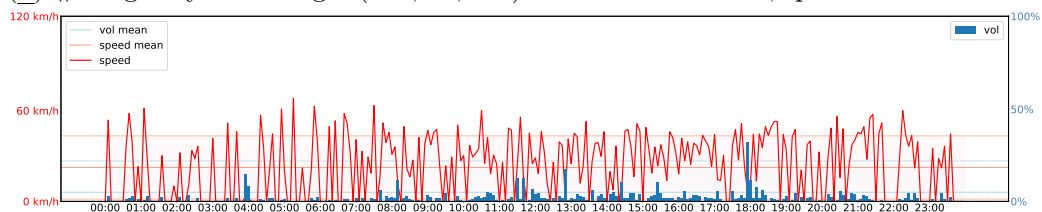
- #1 is a highway in the outskirts has high speed mean and high speed std. This reflects the high speeds during day time and the data sparsity during night time. #1 is close to the 105–125 critical range; it has many no-data points and the average speed is even higher, so every no-data is penalized a lot if the prediction is too high.
- #2 is a main ringroad highway, has high speed mean and relatively high speed std. Although, there is more data in the night, the sporadic speed drops make standard deviation still pretty high. Pretty high free flow speed with a few or no-data points is hard to guess, as every no-data is penalized considerably if the prediction is too high. The zero-volumes during the first hours of the day might be a production artifact, but the location has sparse traffic during the night in all other days we checked.
- #3 is a boulevard in the center of Berlin, which shows that moderate free flow speed and frequent no-data can make the prediction task hard, too.
- #4 is an example from 105–125 speed std critical range, which translates visually into a very spiky speed curve over day. Notice that volumes are low and the spikes mainly come from the no data points. The variance in the speed measurements masked on non-zero volume would be much lower.
- #5 is an example of very low speed std. It shows that there are many directional pixels not or extremely sparsely covered with traffic data, either due to the fleet bias (not covering full traffic) or because there is no traffic in those regions at all.
- #6 is similar to #3, but with slightly higher volumes, lower speed levels and a clearer difference between day and night traffic, which is plausible for a location on the main arteria but not on a highway.



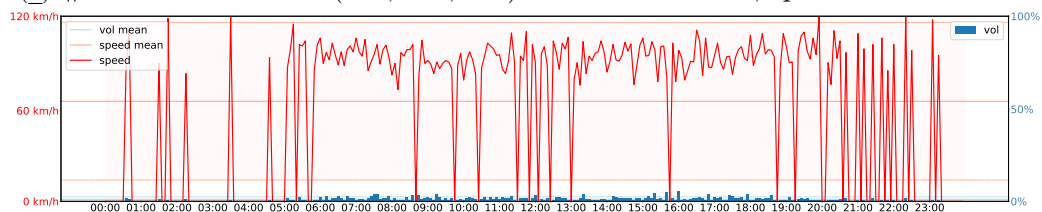
(a) #1 highway outskirts (489, 359, NE). vol: 6.78 ± 6.68 , speed= 186.46 ± 101.55



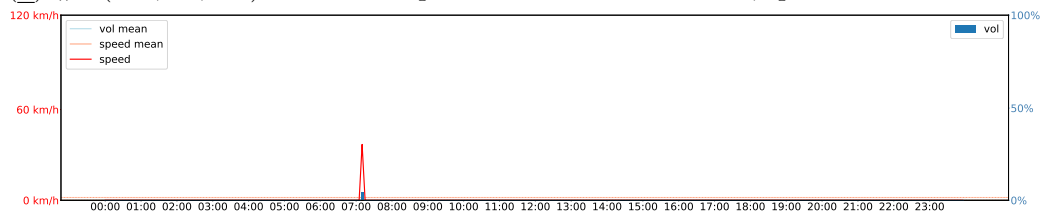
(b) #2 highway main ring. (329, 92, NE). Vol: 16.80 ± 15.112 , speed= 159.69 ± 44.37



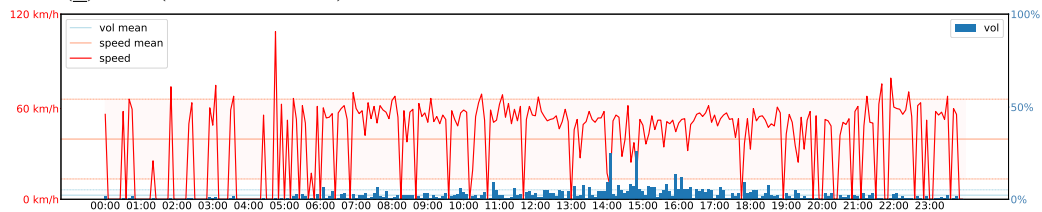
(c) #3 boulevard center (345, 262, NE). Vol: 2.57 ± 43.15 , speed= 46.69 ± 43.56



(d) #4 (494, 62, SE) in 105–125 speed std r. Vol: 2.78 ± 3.48 , speed= 137.87 ± 108.55



(e) #5 (359, 416, SW) with low std. Vol: 0.04 ± 0.73 , speed= 0.23 ± 3.69



(f) #6 (319, 307, NE) in 35–55 speed std r. Vol: 5.67 ± 7.35 , speed= 82.94 ± 54.94

Figure 21: Data from one day in the target domain of the core competition for the 3 Berlin locations and 3 sampled for low speed std, and the two critical speed std ranges. Speed curve in red and volume bars in blue, along with mean lines and std hulls, mean and std from all test slots of the core competition (input and ground truth).

B.2. Relating vol variance to vol MSE

The corresponding plot for volumes is Figure 22.

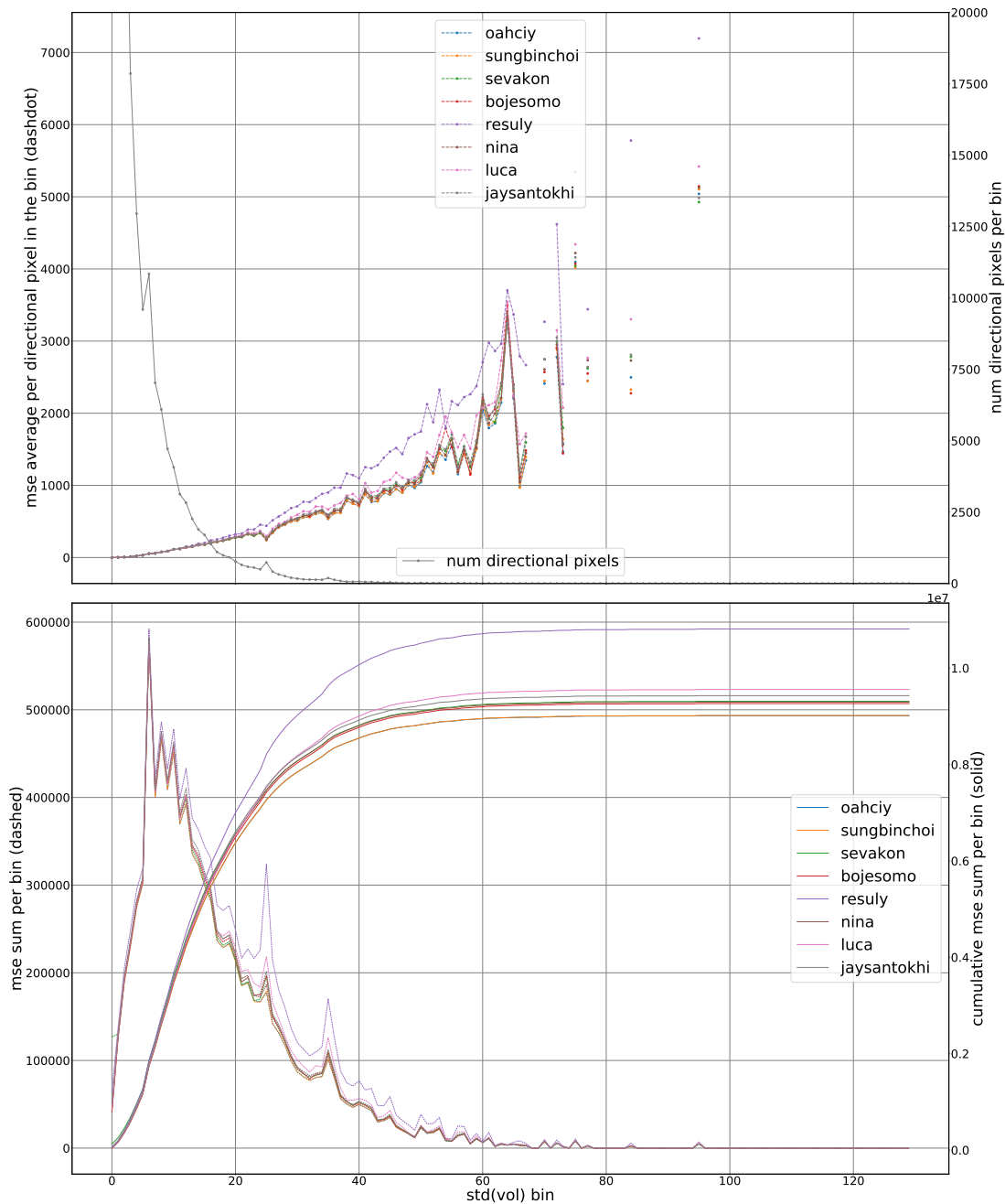


Figure 22: Relating MSE to std for volumes: distribution of std among oriented pixels and average MSE (top); summed MSE and cumulated summed MSE (bottom). The shaded gray areas highlights the two critical speed std ranges.

B.3. Limitations of the analysis and future work

As remarked in Section 3.2, MSE does not optimize each directed location independently, so the interpretation here has to be taken *cum grano salis*. Despite this limitation, we think it is important to relate

- the binning of the directional pixels is based on std in the test slots (input hour and ground truth predictions), it should be checked whether this binning is robust when taking not only the sampled data for the test slots;
- conduct the analysis for other cities as well;
- in the analysis, the mean or percentiles in the data should be taken into account to put the interpretation of related the traffic patterns onto a more solid basis;
- in the same spirit, the analysis should be carried for day and night time separately and compared to the full day.
- In addition to looking at raw MSE values, it might also be interesting to calculate the per-pixel R^2 values for different models.

Appendix C. Outlier Special Prize

Here, we give more details on the Outlier Special Prize introduced in Section 3.4.

C.1. Outlier Special Prize

Quality of traffic prediction heavily relies on the performance in anomalous situations. We aim to have a first look at how models from the t4c21 perform in those situations, both quantitatively as well as qualitatively. Even without sparsity due to vehicle fleets nor daytime nor regional sparsity, outliers are rare in the data and hence MSE does not give a lot of weight to them. Also, typically there are many plausible future scenarios in an outlier situation with a fat tail of scenarios. We invited all Summit/Symposium Participants of *Traffic4cast* 2021 to re-run their models on a new test set for the *Traffic4cast* 2021 Outlier Special Prize. Every participant was allowed to submit two predictions: one with the "plain vanilla" model, as used for the original submission, and one with further training applied. The score was not disclosed to the participants and re-submission was not allowed. The participants were asked to make a prediction on the full without disclosing the outlier location nor the heading. As in the core and extended competitions, only time of day and day of week were disclosed. Also, we did not disclose whether the new slots would be before or after the Covid shift.

C.2. Outlier Heuristics

We tackled outliers in a very pragmatic way. We were not interested in a general definition of outliers, but very much in finding some examples and plot what the models predict in these situations. The outcome of a few trial-and-error iterations was a heuristic that finds outlier situations in a single directional cell.

We compute quantiles on the data for each pixel and each channel separately and use them for a lower and an upper threshold criterion, respectively. Also, in order to focus on situations where a continuous flow is held down by some jam situation, we focus on 8am to 8pm. In order to exclude situations too short to be sure whether they are false positives, we search for situations where the above criteria hold for at least two consecutive time bins. And finally, we take also the 2h mean speed and mean volume into consideration. We choose outlier situations from 9 Tuesdays in September and October 2019 and two cities from the core competition (Berlin and Istanbul, 100 tests for each city). This should give us situations without temporal shift with respect to the training data, neither due to Covid nor due to summer holiday.

In summary, we search and select pixels (just one speed and volume channel) using the following conjunctive filter criteria:

1. volume and speed quantiles (volume above 90% quantile, speed below 5% quantile) and volume threshold (volume above 5)
2. time between 8 A.M. 8P.M.
3. outlier duration (at least two consecutive time bins)
4. outlier mean volume and speed (outlier mean volume above 1.5 times 2h mean, outlier mean speed above 0.7 times 2h speed mean)

These criteria might be highly redundant and we did not check for a minimal set. These criteria are supposed to give us situations where volume is high and speed is low in contrast to normal situation as reflected by full-day quantiles and 2h means and which are robust (two consecutive positives and excluding sparse situations during night time). Formally, an outlier is a quintuple (row, column, heading, start time of day, duration).

For each test, we keep a mask that evaluates MSE on one pixel and two channels, the volume and speed channels of the outlier heading.

C.3. Test Slot Distribution

The procedure just described was applied on 9 Tuesdays in September/October 2019 before Covid temporal shift. Due to data scarcity, the above criteria were not applicable to Chicago and Melbourne from the core competition, so we excluded them as we were interested in the qualitative analysis of the situations. We randomly sample 100 outliers situations per city from 559 (Berlin) and 1266 (Istanbul). The other two cities of the core competitions turn out not to match the pre-conditions of the heuristics and are not included in the Outlier Special Prize. We generate tests such that the first outlier time bin is the last bin of the 1 hour test input window.

The spatial and temporal distribution of the slots are shown in Figures 23–24, respectively. As expected, the spatial distribution is concentrated along main arteries with continuous flow, and the temporal distribution reflects the morning and afternoon peak hours.

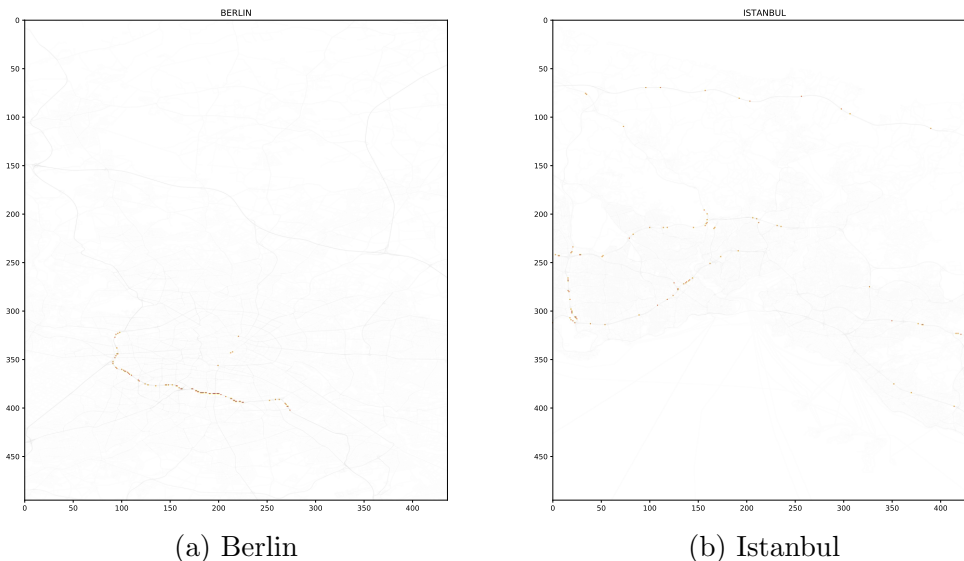


Figure 23: Spatial Distribution of Special Prize Tests.

C.4. Outlier Special Prize Submissions and Leaderboard

We invited all Summit/Symposium Participants of *Traffic4cast* 2021 to re-run their models on a new test set for the *Traffic4cast* 2021 Outlier Special Prize, and from 8 summit participants invited, 7 participated with a total of 11 submissions. 4 participants submitted the solution from re-running their core competition best model, but also submitted a second solution:

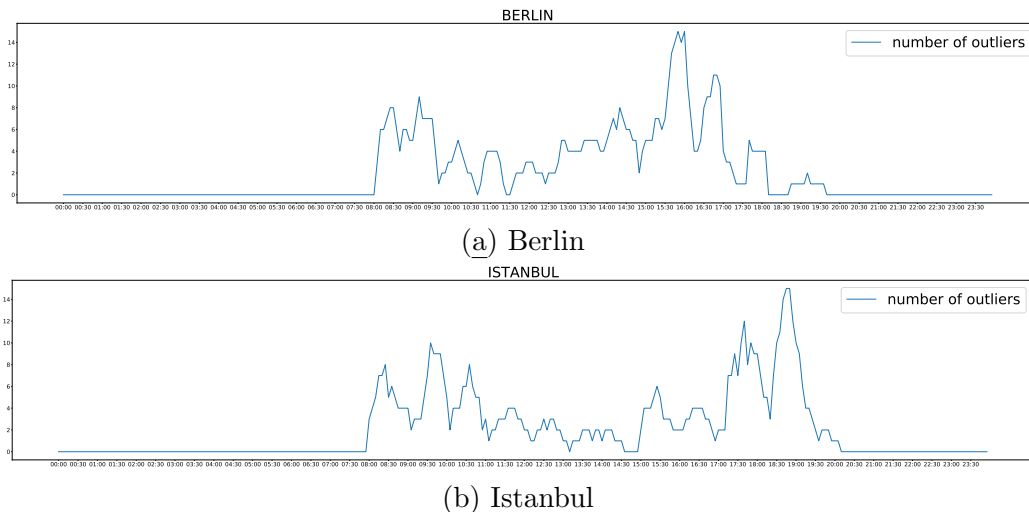


Figure 24: Temporal Distribution of Special Prize Tests.

oahciy_v1 is obtained by exactly the same models that as for the core competition (Lu, 2021).

oahciy_v2 is obtained by further fine-tuning the models for 1 epoch on BERLIN and ISTANBUL data only.]

ai4ex_36 Epoch=36: This is exactly the submissions for the competition (plain vanilla) (Bojesomo et al., 2021).

ai4ex_43 Epoch=43: further training the model.

nina_orig the predictions of the original model (Unet++ patch-based prediction with 100x100 patch and stride s=10 as explained in (Wiedemann and Raubal, 2021)).

nina_special trained the original model further on the two cities separately. In detail, they loaded the model weights, then trained for 500 further epochs on Berlin, and predicted the values for the new Berlin test set. Same for Istanbul (starting again from the weights of the original submission).

sungbin_1 is from best run models on core task (Choi, 2021).

sungbin_2 is from best run models on extended task with different training methods which had not used in the core task (data augmentation method: input image flipping).

The other 3 submissions are jaysantokhi (Santokhi et al., 2021), GraphUNet_luca (Hermes et al., 2022) and Bo (Wang et al., 2021a).

For each test, we keep a mask that evaluates MSE on one pixel and two channels, the volume and speed channels of the outlier heading, see Figure 25. Hence, the quantitative evaluation takes place on much less data than the full city (as in Figure 26): We observe that oahciy_v2 (Lu, 2021), sungbin_1 (Choi, 2021) and oahciy_v1 (Lu, 2021) are very close on masked MSE. Surprisingly, sungbin_2 (Choi, 2021) based on the winning extended challenge

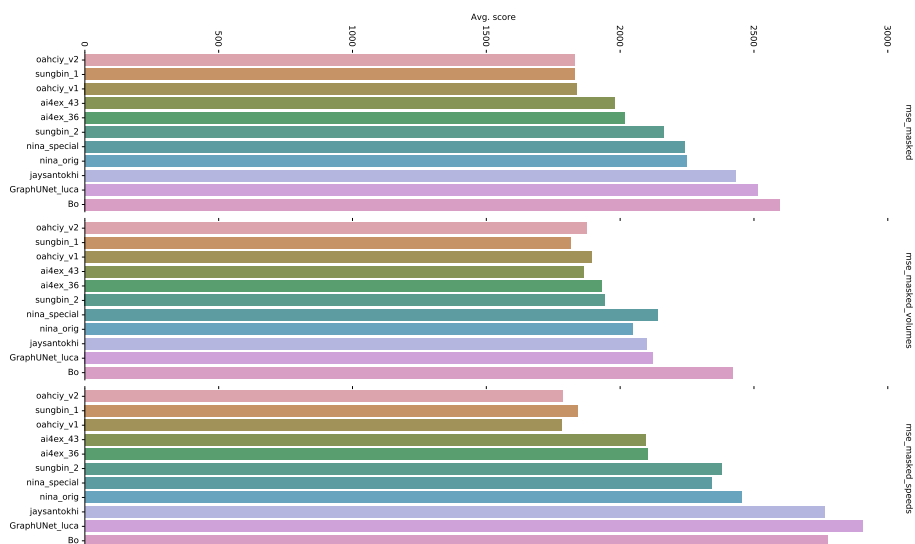


Figure 25: Leaderboard special prize (anomalies) based on masked MSE highlighting one cell and one heading.

is much poorer than sungbin_1, so it seems that sungbin_2 is too “conservative” in this setting where the best guess in most situations is predicting a normalization of the situation. The solutions ai4ex_43/aiex_36 (Bojesomo et al., 2021), nina_special/nina_orig (Wiedemann and Raubal, 2021), jaysantokhi (Santokhi et al., 2021), GraphUNet_luca (Hermes et al., 2022) and Bo (Wang et al., 2021a) are clearly beaten in the Special Prize challenge as well.

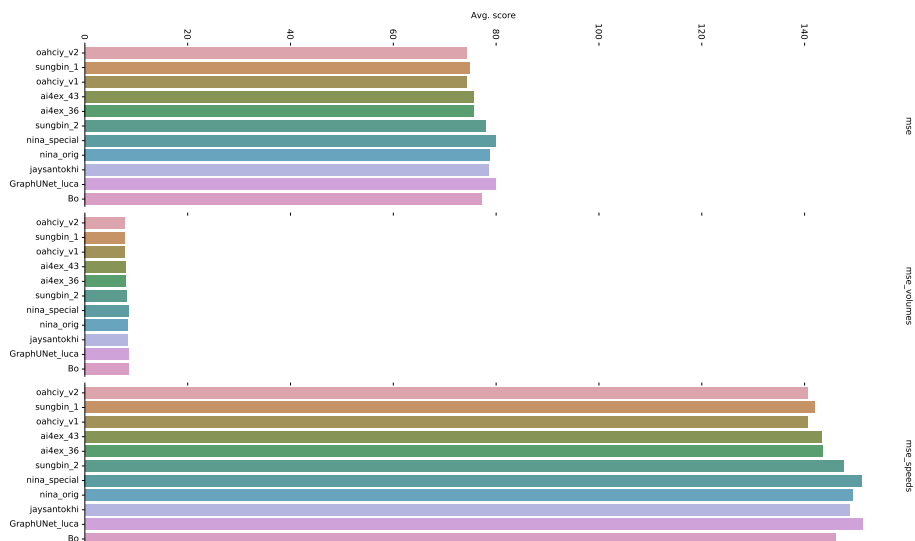


Figure 26: Unmasked MSE in special prize (anomalies) based on masked MSE.

As a sanity check, Figure 26 shows the unmasked MSE, which again shows similar level of MSE overall and for volume and speed separately as in the core competition. We see here the same top-3 submissions as in the core competition (oahciy_v1 marginally better than

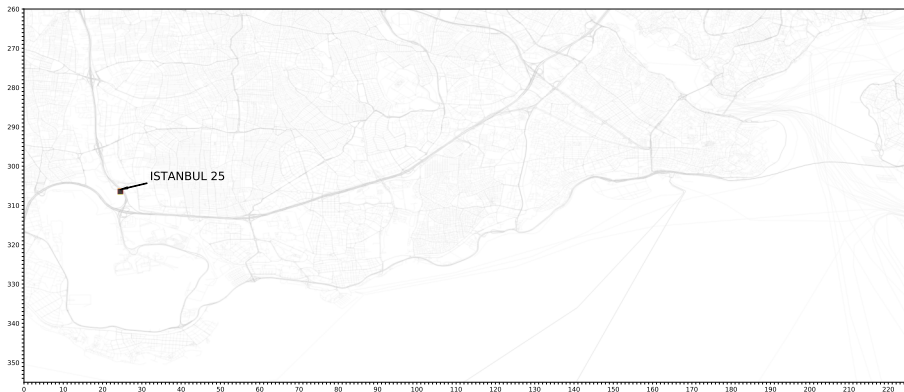
oahciy_v2, Sungbin_1, ai4ex_36, the third prize winner did not participate in the Special Prize). Sungbin_2 trained for unseen cities is clearly inferior to Sungbin_1 in both evaluations.

C.5. Special Prize Qualitative Analysis

Out of the 200 tests (100 for Berlin and Istanbul each), we choose 4 sample situations (see the outlier locations in Figure 27 and describe the anomalies qualitatively:



(a) Berlin



(b) Istanbul

Figure 27: Sample situations

BERLIN 00 Figure 28 : the anomaly started 40 minutes before, stop and go during input hour, normalizing in prediction hour after 10 minutes. We see speed drops during the night and in the evening due to zero volume. The outlier is in the afternoon peak. Prominently, speed has gone down and volume has gone up. The prediction seems to go beyond the mean speed and volume in the input, approximating normalization to “free flow speed”. The highlighted gray area seems to be only at the second half of the jam. However, there was already a partial resolution of the jam, hence our outlier detection heuristic detected two consecutive outlier and we see only the second sampled here. The winner prediction (oahciy_v2 (Lu, 2021)) suggests a steady normalization of volume and speed.

BERLIN 02 Figure 29 unsteady flow during input hour, anomaly started 5 minutes before: peak just before prediction start, normalizing over 30 minutes

BERLIN 97 Figure 30: anomaly 15 minutes before, the jam does not fully resolve during the prediction horizon and we suspect multiple minor go and stops during the prediction horizon (there are two volume peaks in the prediction horizon with low speeds at the same time, which of course could be due measurement error), with speed going up only slowly at the end of the prediction horizon. In this case, the model again predicts a smooth normalization, but far too soon. If we look at the full day ground truth, however, we see that the jam resolved shortly after the prediction horizon, so in some sense the model anticipated that with one smoothed idealised guess, reflecting multiple scenarios only in a statistical sense.

ISTANBUL 25 Figure 31: slowdown started 30 minutes before, going back to normal over 30 minutes

Without a quantitative verification, Figures 28–31 seem to suggest there are 3 typical behaviours:

monotonic normalization The first type is a monotonic normalization to close to free flow speed as in the two examples shown. This is the normal red level we see before the anomaly starts on the left. And the dashed red line gradually creeps back to that level over the one hour prediction horizon left to the vertical now line. The same happens for volume (blue) which goes down when the jam resolves. However again, the prediction does not fully recover so the model probably learns from the training data to expect to expect not full resolution of the jam over the prediction horizon. They seem to provide a “smoothing” of the anomaly going back to normal. Clearly overestimating in Berlin 97, where the situation does not normalize during the prediction horizon.

monotonic towards mean of input The second class does predictions which are monotonic towards mean of input. The mean of the input is shown by the faint horizontal red line. So it looks as if in these cases only consider the local effects in the input.

static The third class does a jump and stay prediction. Some models jump to the mean speed of the input as in the example shown on the right-hand side. Other models of the third class jump even to something close to free flow speed.

All models seem to predict pretty high volumes from what we would expect as the non-jammed normal volume from the input hours in the left half of the plots.

In summary, the best models predict smoothed version of a jam resolution (Berlin 00), underestimating speed and overestimating density; models are fooled in case jam does not resolve (Berlin 97), MSE makes prediction blurred towards the mean in the data, never predicting a rare scenario such as jam resolving more or less quickly than in expectation; MSE for volume and speed is at the same level.

We do not provide a thorough and systematic exploration of this classification, but we think it still illustrates some shortcomings of the current task formulation discussed in the main text.

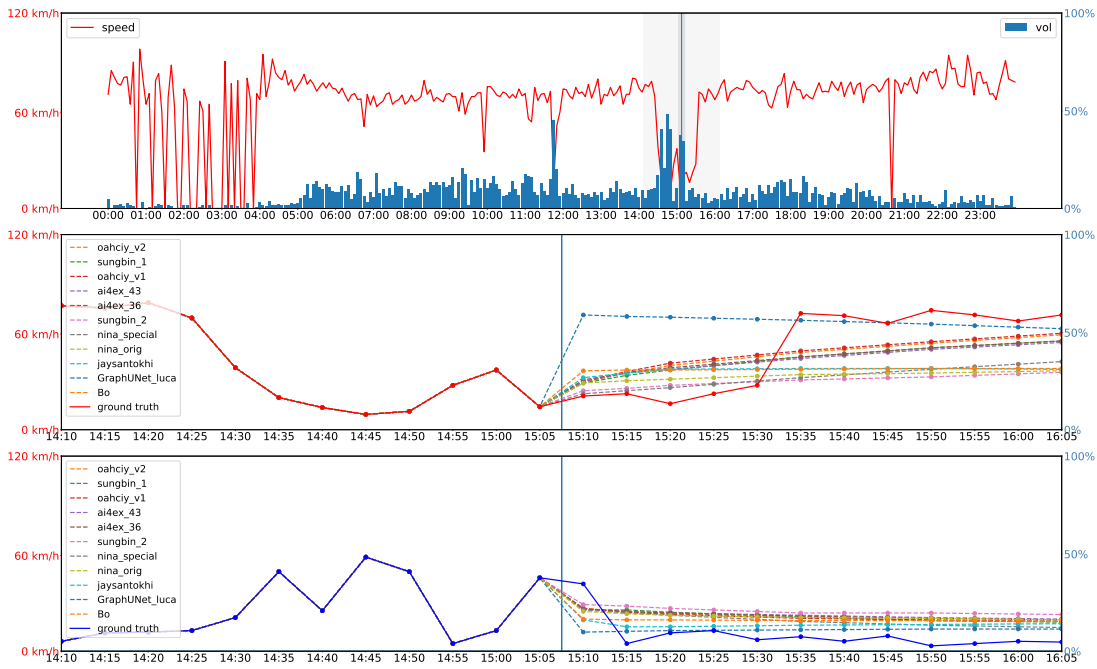


Figure 28: Predictions Berlin 00. Top: Daytime curve of ground truth data for 288 bins from midnight to midnight with speeds (red curve) and volumes blue bars. Outlier in darker gray area with input and prediction hour in light gray separated by a blue vertical line. Middle, bottom: The dashed lines show the speed and volume predictions of the different submissions compared to ground truth (solid lines); the vertical blue line separates input from output in time.

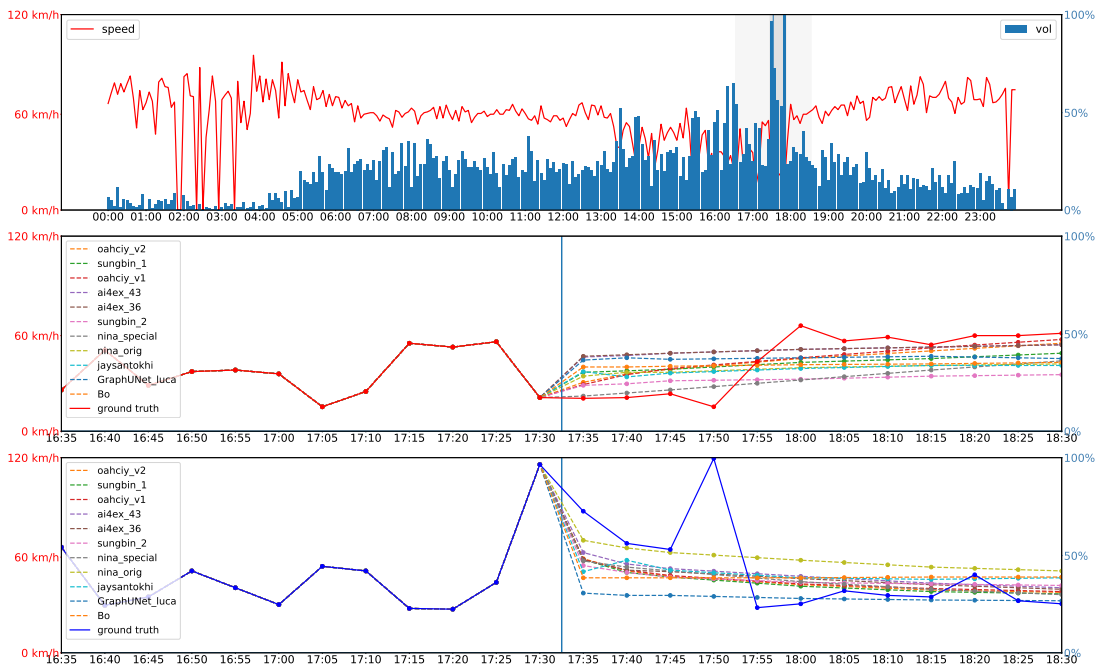


Figure 29: Predictions Berlin 02

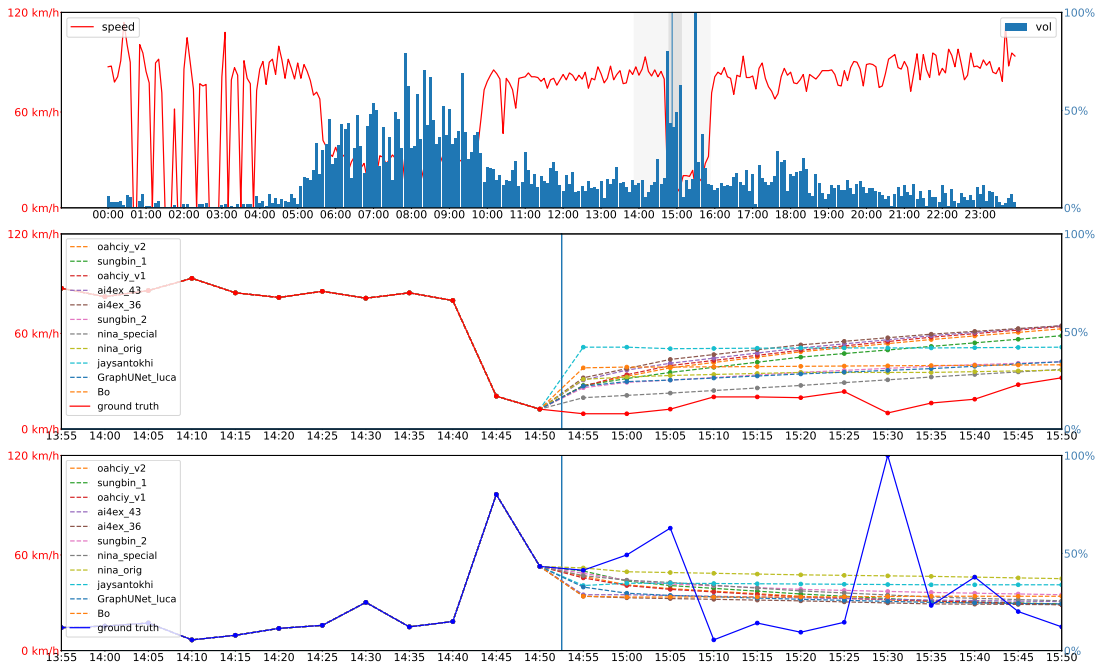


Figure 30: Predictions Berlin 97

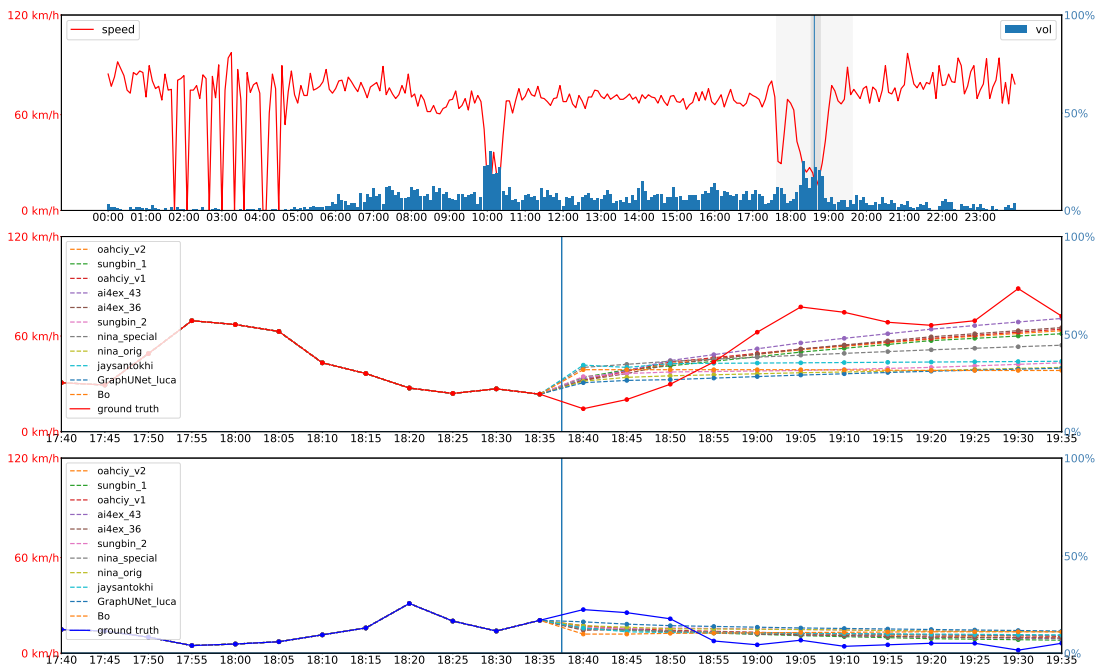


Figure 31: Predictions Istanbul 25

Appendix D. Leaderboards Core and Extended Competitions

In this appendix, we highlight some aspects of the leaderboard to highlight some features of MSE evaluation in the *Traffic4cast* setting. The code used to generate them and more plots can be found in (Eichenberger and Neun, 2021).

Figure 32 shows the dominance of speed channels in both competitions.

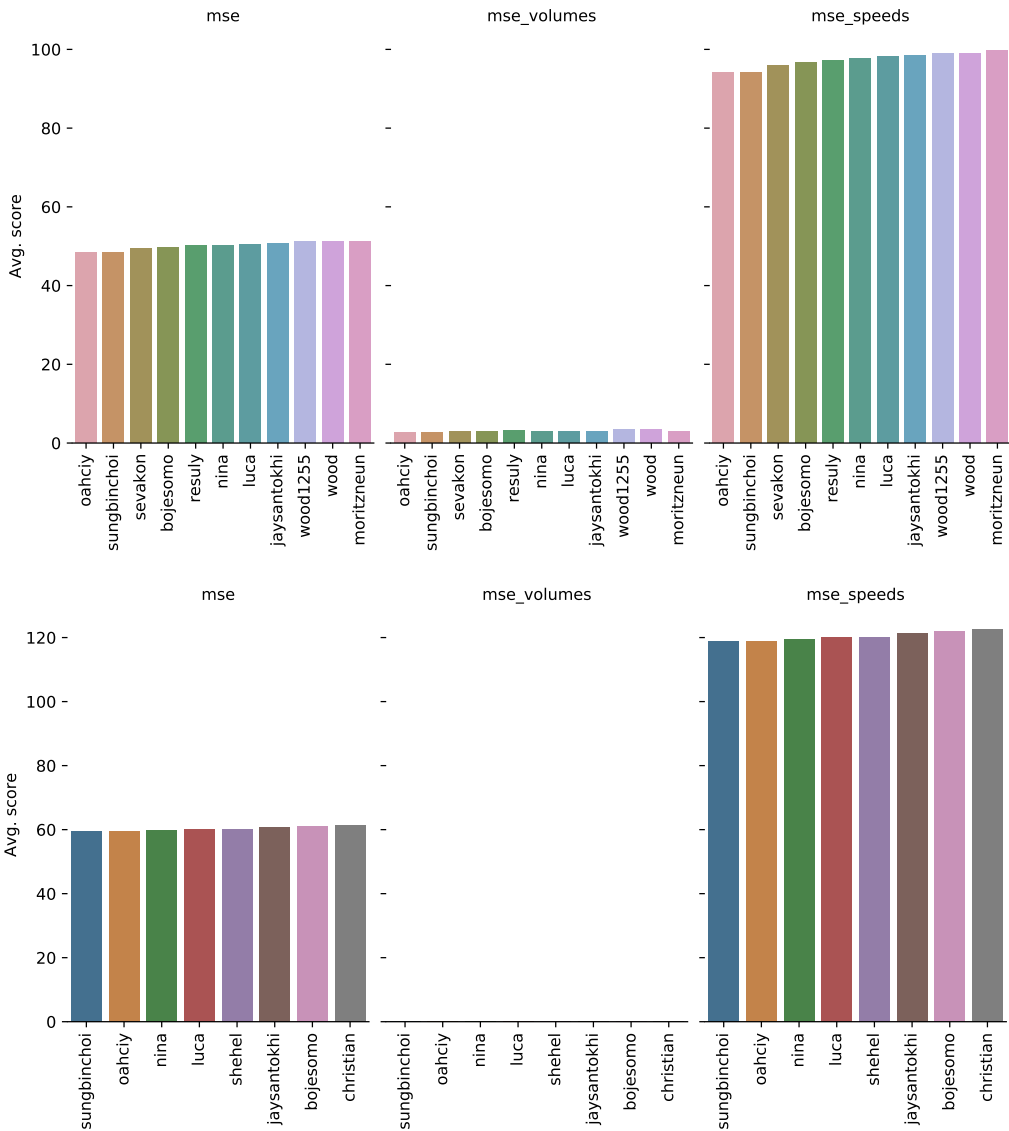


Figure 32: MSE Volume vs. speed bias: MSE over all channels and MSE on volumes and speeds separately for core competition (temporal shift, top) and extended competition (spatio-temporal shift, bottom). MSE is the average of volumes and speed MSE by definition.

Supplementary Material

Appendix E. Design of *Traffic4cast* 2021

In this Section, we motivate the design of *Traffic4cast* 2021, referring to past *Traffic4cast* competitions and to the scientific literature.

E.1. Background and Motivation

Since 2019, our *Traffic4cast* competition series at NeurIPS has contributed both methodological and practical insights, advancing AI-driven traffic forecasting and research on the general applicability of the resulting methods to predicting other spatial processes. Although such traffic forecasts are thought to form the basis for building and managing our cities to provide efficient and sustainable mobility (Bucher et al., 2019; Jonietz et al., 2018; Lee et al., 2018), this form of traffic prediction is still largely considered to be an unsolved problem (Guo et al., 2019a).

In our first edition of *Traffic4cast* competition at NeurIPS 2019, we encouraged contestants to predict traffic flow volumes, velocities, and dominant flow directions 15 minutes into the future on a unique, large, real world data set (Kreil et al., 2020). A key innovation of our *Traffic4cast* competitions was the chosen representation of traffic: we aggregated the data from individual sensor measurements in space and time bins. The values of the spatial representation of each time bin could be interpreted and visualized as a ‘movie’ frame, thus effectively recasting the traffic prediction task as a video frame prediction task (see (Kreil et al., 2020; Kopp et al., 2021)). These Traffic Map Movies, for the first time, provided a high resolution privacy preserving comprehensive view of urban traffic. The design of the 2021 competition was built on the success and insights already achieved so far (*cf.* Section E.3). In a nutshell,

1. Our chosen representation was highly effective and – as independent work has shown for precipitation prediction (Agrawal et al., 2019) – should be considered a promising new technique for tackling complex geo-spatial processes.
2. Our 2020 competition asked participants to predict traffic in the second half of 2019 from given data in the first half of 2019. Thus temporal transfer learning across seasons was possible, although a performance boost could be achieved when also using the validation set data provided for training (Qi and Kwok, 2020).
3. The work of Martin et al. (2020a) following their 2019 prize winning solution indicated that some degree of transfer of learned traffic patterns to almost unseen cities was possible with their GNN approach.

E.2. Competition Tasks and their Academic and Real-World Applications

Going beyond the challenges at NeurIPS 2019 and 2020, the 2021 edition explored models that adapt to domain shift both in space and time, focussing on the question of model robustness and generalizability across time and space, even if this involves a clear domain shift – as in moving from one city to an entirely different city, or in moving from pre-COVID

times to times after COVID hit the world. The change in mobility even in partial lock-downs is well-documented (Google; Li et al., 2021; Strava), and we know from colleagues in city governments that classical traffic models struggled with the drastic changes, a general well observed and explored phenomena in machine learning (Ben-David et al., 2010; Wouter, 2018; Kouw and Loog, 2019; Webb et al., 2018; Gama et al., 2014; Widmer and Kubat, 1996). The question arises how much better data driven models can perform. We compiled an order of magnitude more data that covers 10 cities across 2019 and 2020, giving us the flexibility to explore this question on a unique, diverse real-world data set. We did complement these dynamic data by static information on road geometry.

With that we provided two challenges to participants:

- In the **core challenge**, participants were tasked to handle temporal domain shift (an active field of machine learning research (Ben-David et al., 2010; Wouter, 2018; Kouw and Loog, 2019; Webb et al., 2018; Gama et al., 2014; Widmer and Kubat, 1996)) in traffic due to COVID-19. In addition to the full data for four cities described, participants received pre-COVID data for four further cities, *plus* one hundred 1 h slots from 2020 after COVID struck. The challenge then was to predict the dynamic traffic states 5, 10, 15, 30, 45 and 60 minutes into the future after each of the one hundred time slots for each of the additional 4 cities.
- In an **extended challenge**, participants were asked to again predict dynamic traffic states for two further cities, for which provided only static road geometry. Like for the first challenge, traffic needed to be predicted 5, 10, 15, 30, 45 and 60 minutes into the future following 100 given 1 h time slots. Yet there was no further traffic data provided for these cities. Moreover, for each city, 50 of these 100 1 h time slots were from the period before COVID, and 50 from the period after COVID, without revealing which!

Our **core challenge** dealt with the real world problem of developing a new model or adapting an existing model to be robust to temporal domain shifts. Our competition allowed us to study this directly by providing data from pre-COVID times *vs* in-COVID times for the same locations for training. The few-shot transfer learning task then was to successfully apply these models to a new city, with full data for the pre-COVID period but just a few input samples from the in-COVID period. Our **extended challenge** increased the complexity of the goal by providing no large-scale training data for the new test cities at all. Models thus needed to handle both spatial and temporal changes in the data guided by only a few example measurements from the test set. Solutions to both problems are of direct importance to real world traffic prediction and for effective city planning.

We note that a solution to the ‘extended challenge’ could also be applied to the ‘core challenge’, thus truly making it more universal. Both challenges are few-shot learning challenges, an actively developing area of AI (Ben-David et al., 2010; Fei-Fei et al., 2006; Lu et al., 2020; Guo et al., 2019b), and could be tackled in a multitude of ways given the data provided. The common underlying scientific question is how to build robust models that can predict how a complex spatial process evolves over time, so that the models can swiftly adjust to domain shifts (Ben-David et al., 2010; Wouter, 2018; Kouw and Loog, 2019; Webb et al., 2018; Gama et al., 2014; Widmer and Kubat, 1996) both in space and time after seeing only a few examples from the new regime.

Moreover, the ability to quickly adapt existing models to temporal domain shifts is a key concern in real world applications more generally, many of which are critical to the functioning of our society. Solutions of our *Traffic4cast* competition so far seemed to generalise well to other geo-spatial processes, when aggregated similarly in space and time (such as seen for weather (Agrawal et al., 2019; Herruzo et al., 2021; Gruca et al., 2021), cf. <https://weather4cast.ai/> at CIKM and IEEE Big Data 2021). Approaches developed in our competition can thus have a similarly profound impact there. Moreover, the emergence of novel approaches to key questions on model stability, adaptability, and transferability will in itself constitute a critical advance towards tackling some of humanity’s largest problems. The clear connection of the *Traffic4cast* challenges to real world scenarios, the large-scale nature of the underlying data used, and their direct appeal addressing classic AI research questions were aiming at highly topical fields of few-shot and transfer learning, meta-learning more generally, graph based modelling, deep learning, and video frame prediction.

In the traffic domain, this has direct substantial implications for city planning, as first order effects of road closure or building new roads could be tackled from a data-driven perspective. Being able to infer the traffic states of hitherto unseen cities from few observations would open the door to offering accurate traffic predictions at much lower computational cost, in more places, ultimately being able to work with more diverse, non-recurrent, data sources. This is of particular importance to cities in developing nations. Thus, even only considering the impact on traffic, our competition will have a large impact on how we design our future way of living (societal), on our ability of how we can plan our mobility needs (economical), and our ability to provide these key services to everyone at minimal cost (humanitarian).

E.3. Additional Competition History and Insights

Video prediction is a highly active field with promising distinct approaches (Han et al., 2019; Kwon and Park, 2019; Lee et al., 2018; Oprea et al., 2020; Srivastava et al., 2015; Walker et al., 2016; Xue et al., 2016) which we hoped could be harvested by the traffic prediction community as well.

Our 2019 competition yielded the following insights (Kreil et al., 2020):

- Re-phrasing traffic forecasting as a video prediction problem turned out to be of merit and – as independent work has shown on precipitation prediction (Agrawal et al., 2019) – should be considered a promising new technique in tackling complex geo-spatial processes. Capturing the complex spatio-temporal dependencies of such processes is known to be a hard problem, usually referred to as ‘spatial is special’ (Anselin, 1989), and our 2019 competition contributed evidence that neural network techniques in this simple video frame prediction setting yield promising results.
- Anecdotal evidence stemming from the attempt by some contestants indicated that trying to add additional prior static or dynamic location knowledge about the spatial bins did not seem to improve results significantly (Martin et al., 2019; Herruzo and Larriba-Pey, 2020), suggesting that such information was already encoded in the complex traffic data itself. Moreover, no successful strategies in our competition used recurring traffic patterns based on time of day or day of week, which would have been

possible in the competition design, providing further anecdotal evidence that traffic is ‘quasi-markovian’, *i. e.* mostly dependent on the immediate past only.

- Most successful solutions indicated (Choi, 2019; Martin et al., 2019; Yu et al., 2019) that our discretized ‘majority heading’ channel was the least informative and was also hardest to predict.

Given the unexpected success of phrasing our traffic forecasting problem as a movie prediction task, we decided to maintain our simple spatial and temporal aggregation approach for the *Traffic4cast* competition at NeurIPS 2020 and examine further some of the findings while challenging our assumptions in the design of the first competition:

- We decided to double down on the implicit question thrown up by Martin et al. (2019) and Bucher et al. (2019) of whether additional static and dynamic data potentially relevant to the geo-spatial process of traffic could improve predictions. This question was heavily explored by our contestants. There is anecdotal evidence (Kopp et al., 2021) that especially the provided incidents information was of little help.
- The literature presents empirical evidence that the performance of numerous traffic prediction models would typically decrease significantly past a 15min horizon, and a majority of studies of ‘short-term prediction’ thus focus on such time horizons (Ermagun and Levinson, 2018a; Dunne and Ghosh, 2011; Ermagun and Levinson, 2018b; Lana et al., 2018). In line with common practice, we therefore restricted our 2019 competition to that horizon. After these initial experiences, in our 2020 competition we extended the horizon to 60min into the future and the results point to a strong affirmative answer as similar and improved architectures from the 2019 competition (*e. g.* (Choi, 2020; Wu et al., 2020)) showed little deterioration over the longer time horizon.

Moreover, (Qi and Kwok, 2020) reports that merging the results of a U-net architecture (Ronneberger et al., 2015) with that of a Graph Ensemble Network (GEN) (extending the GNN in (Martin et al., 2020a)) leads to a performance improvement, indicating that their GEN can capture different dynamic aspects to their U-net approach. They argue that in contrast to pure image-based approaches, formulating the prediction problem on a graph allows the neural network to learn properties given by the underlying street network, facilitating the transfer of a learned network to predict the traffic status at almost unknown locations. This last insight, first formulated in (Martin et al., 2020a), lies at the heart of our proposed ‘extended challenge’ for this year’s competition, essentially asking participants to use transfer learning or few-shot learning techniques to use knowledge of existing traffic dynamics in order to predict traffic states at unknown locations.

Appendix F. Competition Data

F.1. Data Provisioning

We provide a unique data set derived from industrial scale trajectories of raw GPS position fixes (consisting of a latitude, a longitude, a time stamp, as well as the vehicle speed and driving direction recorded at that time). The data are aggregated and made available by

HERE Technologies and originate from a large fleet of probe vehicles which recorded their movements in multiple culturally and socially diverse metropolitan areas around the world. The time span of the data covers both the years 2019 and 2020 providing an opportunity to observe the effects of the COVID pandemic in different cities. We provide data for 10 entire cities in different configurations to empower both the temporal and spatial transfer learning tasks. Over 10^{12} GPS points are used to generate the data sets for the 10 cities covering a time span of 2 years.

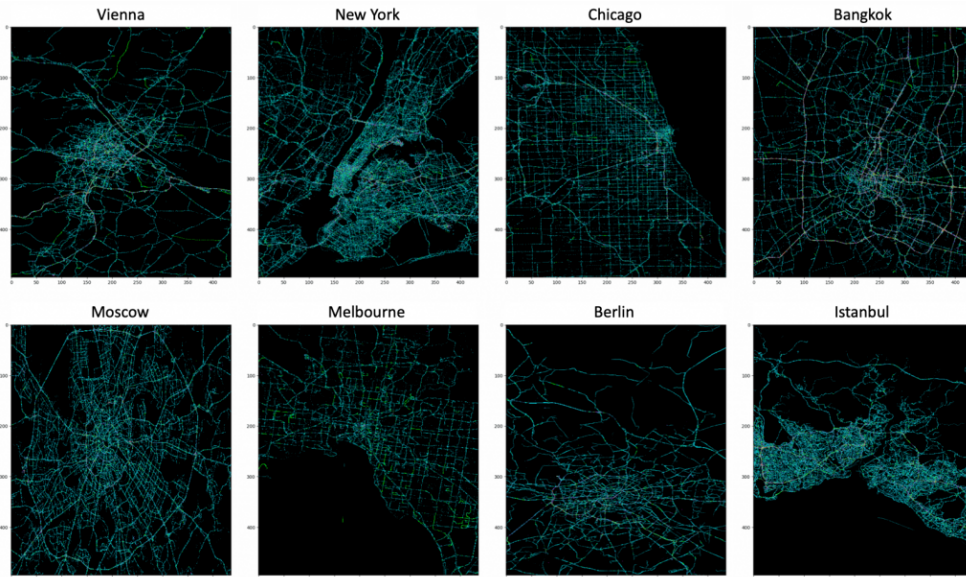


Figure 33: The figure below shows Traffic Movie renderings from 8 different cities highlighting the diversity of locations covered with differences in road network structure, fleet layout and traffic behavior and other cultural effects. Each snapshot covers $\sim 50 \text{ km} \times 50 \text{ km}$ of urban area, with our data thus providing full comprehensive coverage of complex cities. Pixel brightness indicates traffic volume for an area ($\sim 100 \text{ m} \times 100 \text{ m}$) at the time of the snapshot and a 5 minute time bin. We show the sum over multiple channels and multiple time slots. Note, like in previous years, we rotated the data for Moscow by 90 degrees in order to fit the entire city with the enclosing ring road into the traffic movie shape. This has no influence on the prediction

The encoding and aggregation scheme of the shared data is an evolution of the data used in the two previous competitions (Kopp and Kreil, 2019, 2020). In terms of coverage and volume, the amount of data is growing and provides a unique dataset to allow conclusive results. Similarly to the previous years, the data was made freely available for download from HERE Technologies. As also mentioned in the task description Section E.2, we are holding back some time intervals for some cities (core challenge, temporal transfer), as well as most of the data of two further cities (extended challenge, spatio-temporal transfer).

Table 2 gives an overview about how data is used for training and testing of the core and extended challenge: A visual representation of the provisioned data can be found in

cities ↓/data→	static	dynamic			
		training		few-shots/test	
		pre-covid (2019)	in-covid (2020)	pre-covid (2019)	in-covid (2020)
4 (known cities: Moscow, Barcelona, Antwerp, Bangkok)	✓	180 days (24h)	180 days (24h)	–	–
4 (temporal: Berlin, Istanbul, Melbourne, Chicago)	✓	180 days (24h)	–	–	100 (1h)
2 (spatio-temporal: Vienna and New York)	✓	–	–	50 (1h)	50 (1h)

Table 2: Data Provisioning: Training and test data provisioning for 10 cities for *Traffic4cast* 2021. For all cities, a static road graph was provided as well.

Figure 34.

F.1.1. DYNAMIC CHANNELS

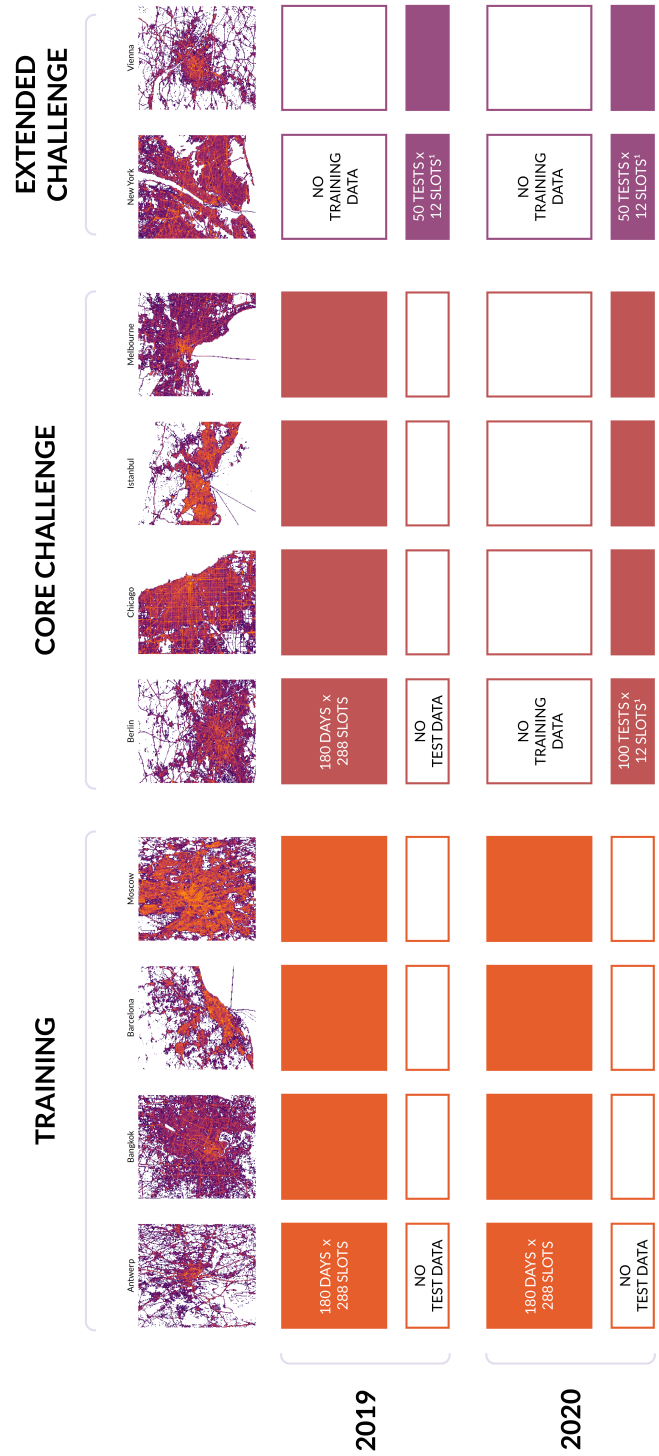
The GPS measurements are aggregated across spatial cells of $\sim 100\text{ m} \times 100\text{ m}$ and over a time-window of 5 minutes. Figure 35 shows a simplified spatial tessellation (left) as well as the actual resolution of a road network illustrating the contents of an example 100×100 cell in a dense city area. The output of this aggregation can be encoded (described below) as an ‘8 channel movie’ with each 5 minute bin representing a time frame and with the densities and other aggregate features of the cells being mapped to generalized pixel values in different channels. Hence, the output is represented as a generalized movie with 288 frames for a single day of one city.

In the *Traffic4cast* at NeurIPS 2020 competition, we extended the GPS feature aggregation from the initial 3-channel (volume, mean speed and main heading) to an 8-channel encoding (see Figure 36), where two features are calculated for each heading direction quadrant of North–East (heading 0° – 90°), South–East (heading 90° – 180°), South–West (heading 180° – 270°) and North–West (heading 270° – 0°):

- Volume: The number of probe points recorded from the collection of HERE sources capped both above and below and normalized and discretized to an integer number between 0 and 255.
- Mean speed: The average speed from the collected probe points. The values are capped at a maximum level and then discretized to $\{1, 2, \dots, 255\}$, by linearly scaling the capping speed to 255 and rounding the resulting values to the nearest integer. If no probes were collected, the value is 0.

This 8-channel representation of dynamic data is backwards compatible and allows for an easy adoption and potential re-use of solutions of our previous competitions.

Unlike in our *Traffic4cast* 2020, neither static POI (point-of-interest) density maps nor the dynamic incident channel (which proved unhelpful to participants, see (Kopp et al., 2021)) were provided. The summary of the channel changes can be seen in Table 3.



¹Given one hour of data in 12 slots of 5min, predict the next 5, 10, 15, 30, 45 and 60 lead times.

Figure 34: Data Provisioning: Training and test data provisioning for 10 cities for *Traffic4cast* 2021. For all cities, a static road graph was provided as well.

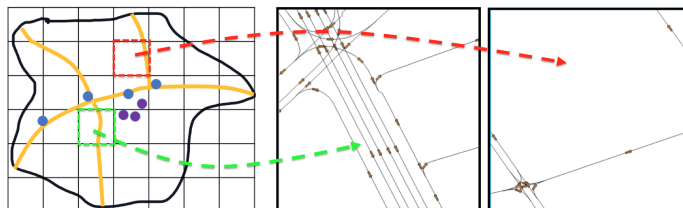


Figure 35: Spatial tessellation of the road network. The left box shows a gridded topology (the yellow lines represent roads, dots symbolize example GPS recording locations, the black contour line outlines the city border). The two boxes on the right show a magnification of two exemplary grid cells to illustrate the contained road network complexity. The two cells are surrounded by green and red dashed square boxes and are related to the two big boxes on the right as indicated by the green and red dashed arrows.

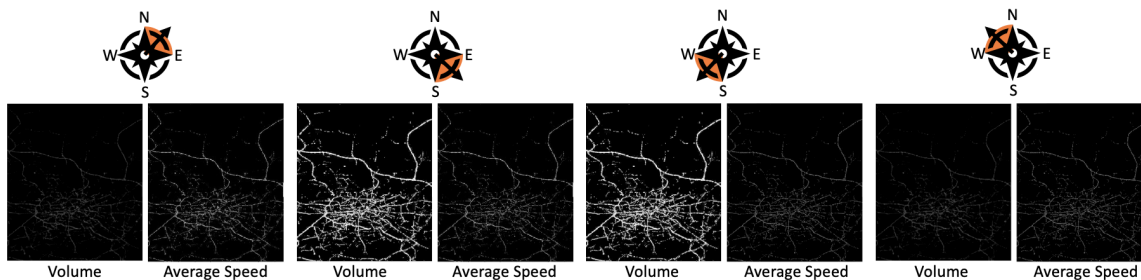


Figure 36: The 8 probe channels, 2 for each heading quadrant.

F.1.2. STATIC CHANNELS

We provided additional static channels in order to encode contextual information about a cell. As in most cities road geometry features at this aggregation level are reasonably static over time, for these channels only a spatial resolution is required.

Instead of the junction cardinality and junction count channel of the previous competition (Kopp et al., 2021), we provided a road map channel which encodes the road geometry connections to the neighbouring cells and their general relative throughput in the present competition. In particular, with regards to the spatial transfer learning component of the 2021

description	<u>d</u> ynamic / <u>s</u> tatic	nb. of channels	2020	2021
volume per heading	d	4	✓	✓
mean speed per heading	d	4	✓	✓
incident level	d	1	✓	×
POIs	s	5	✓	×
junction cardinality and junction count	s	2	✓	×
road map	s	9	×	✓

Table 3: Channels used in the 2020 and 2021 competitions.

competition, it appeared vital to provide such non-local connectivity information to support learning of general, transferable rules, that only rely on standardized, city-independent road features.

The data provided is illustrated in Figure 37:

- a gray-scale representation of the city map in the same resolution as the dynamic data (Figure 37 left).
- a binary encoding of whether the cell is connected to its neighbor cell/pixel to the N, NE, . . . , NW. This connectivity matrix (see a visualization (Figure 37 middle)) has the same resolution as the dynamic data (495,436) but has been derived using a
- finer grained representation as input (Figure 37 right).

The city maps are meant to be compatible to the way how the probe movies are generated. The general aggregation pattern of the data is as simple as using the WGS84 degree coordinates and binning them to 0.001 intervals. Hence, every pixel represents an area of 0.001 by 0.001 degrees. In the text we often refer to this as an $\sim 100\text{ m} \times 100\text{ m}$ area as it is more illustrative, but of course this depends on the latitude (*e. g.* in Istanbul $\sim 111\text{ m} \times 85\text{ m}$, in Berlin $\sim 111\text{ m} \times 70\text{ m}$ or in Bangkok $\sim 111\text{ m} \times 108\text{ m}$). This can lead to the impression of seeing the data stretched/compressed compared to a typical map representation. The variances of real cell sizes between cities are acceptable as the general aggregation scheme is coarse and also does not directly mitigate *e. g.* the error introduced by different GPS populations in different cities having different general accuracies. Within a city, the cells have comparable relative areas and stable neighbourhood relationships.

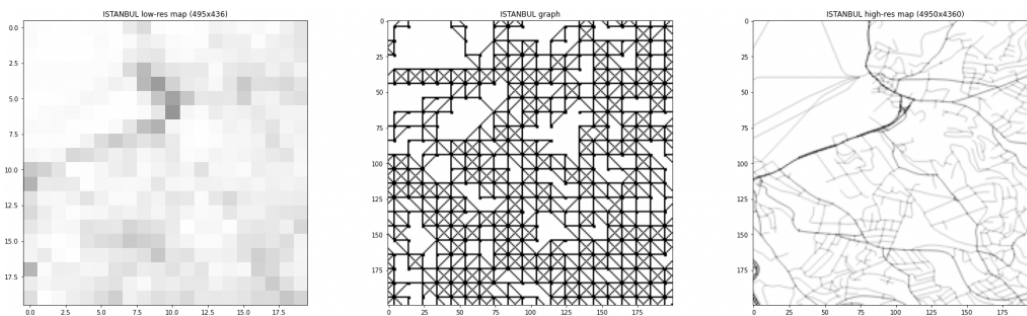


Figure 37: Low-res grayscale (left), connectivity (middle) and high-res gray-scale image(right) for a part of Istanbul.

We will now give more details about the chosen encoding and the creation of the provided connectivity layers. We refer to the 5 steps in Figure 38 and 39 and to the code published in (Eichenberger and Neun, 2021):

1. The source for all layers is a rasterization of the street network to a picture with 4950×4360 pixels for each city. This raster has been generated using road data from HERE Technologies (see step 1 below). The result of this rasterization is provided as the high-res image.

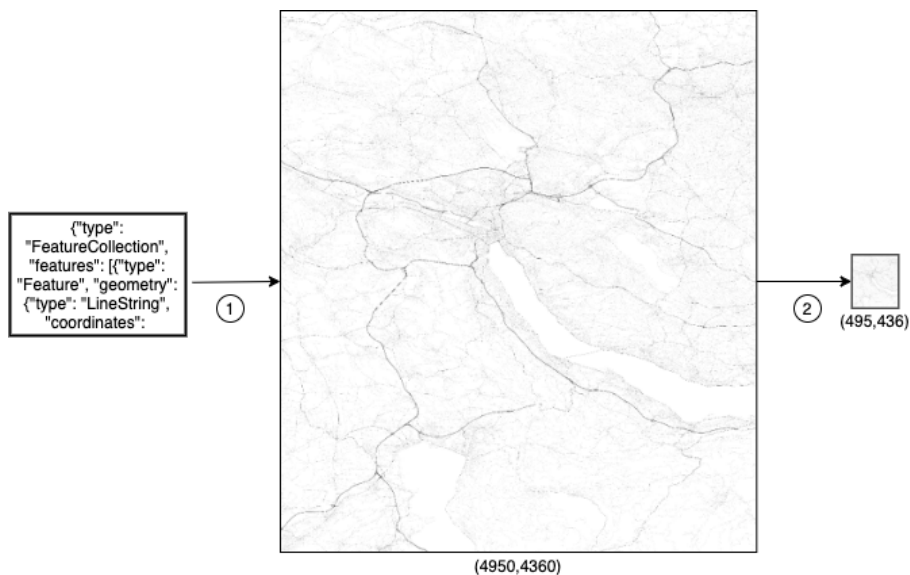


Figure 38: First two steps of static road map generation showing input and output data structures.

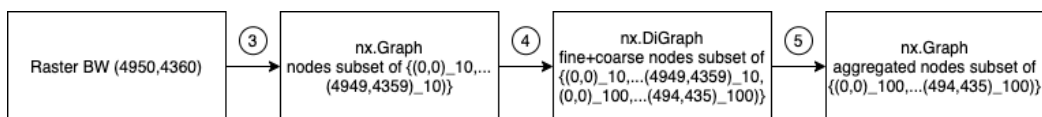


Figure 39: Steps 3–5 of static road map generation showing input and output data structures.

2. We generate a low-resolution raster by downsampling the image to 495×436 . This is the first channel in the connectivity file and just gives a very rough density value for the underlying road network.
3. We then use the high res raster from step 1 to build a “pixel graph” at high-res, introducing edges between non-white pixels (*i. e.* not taking into account gray scales, only “black and white”).
4. After building the raw pixel graph, we introduce edges between the high-res nodes (upper right of Figure 40) and their corresponding low-res nodes (lower right of Figure 40), resulting in a graph with both types of nodes.
5. Additional detour connections at the corners of a pixel are introduced if there is a path of length ≤ 7 . The detours are needed for properly representing the connectivity across the corners in the Moore neighborhood. This is illustrated in Figure 41.

Finally, the plots of Figure 37 show the contents of the resulting delivered static datasets for a slightly larger area. The coarse (low-res) map (right plot) has the same resolution as the dynamic data and can be used directly as a density channel. The high-res map (middle plot) serves as reference to understand the underlying road network and can also be used

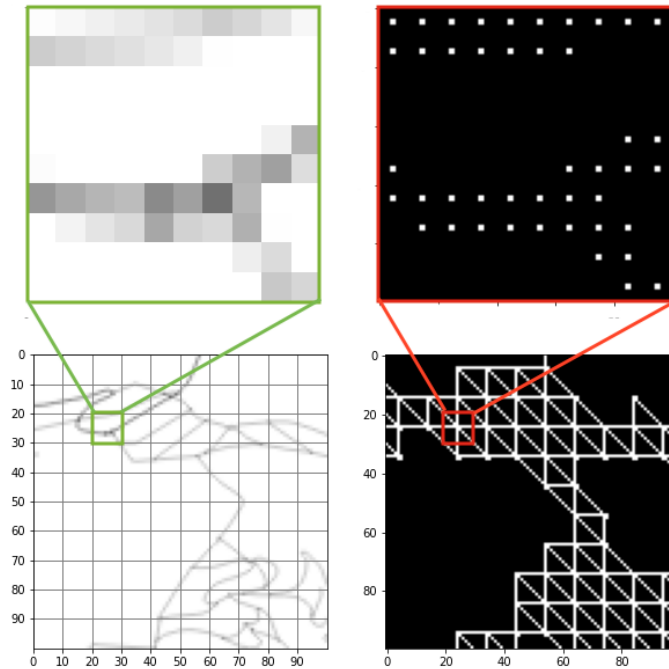


Figure 40: Step 4 of connectivity derivation. Left: gray-scale, right: graph, top: high-res, bottom: low-res. The upper right (red border) shows an extract of the raw pixel graph for a $\sim 100\text{ m} \times 100\text{ m}$ area. Every dot is a node and every node is connected with all its direct neighbors (edges not visualized). In the upper left (green border), the magnified contents of the high res map raster image are shown. In the lower left corner, the larger context and road network in a 1 km^2 area with the target node resolution 495×436 . The green and red lines show the locations of these two extracts in the low-res representations.

freely to derive other representations for solving the competition challenges. The 8 channel connectivity graph data (visualization in the left plot) represents the direct neighborhood relationships for every cell in the same resolution as the dynamic data. This representation is richer (see *e.g.* the detours above) than the plain rendering of the low-res raster map and can be used more flexibly.

F.1.3. TRAINING DATA FORMAT

Data was made available in HDF5 format of 2 different types:

static The static part for a city consists of a $(9,495,436)$ tensor and a $(4950,4360)$ tensor of higher-res gray-scale map where each pixel corresponds to $\sim 10\text{ m} \times 10\text{ m}$, and it is easy to map the pictures by factor 10. In fact, the lower-res map (first channel) is a down-sampled version of this higher-res map, and participants could generate their own static encoding at the prediction resolution. The first channel is a gray-scale representation of the city map in the same resolution as the dynamic data. The other

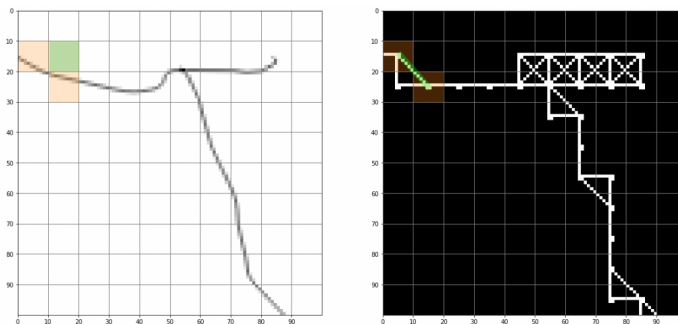


Figure 41: Adding detours in step 5 of the connectivity derivation. Orange cells are not directly connected in the road graph but depending on the frequency a GPS point very well could move “directly” between them. Hence, there is a connection via the green cell added.

8 layers are a binary encoding of whether the cell is connected to its neighbor cell/pixel to the N, NE, ..., NW.

dynamic The dynamic part of the training set consisting of 180 dynamic layer files (h5) each containing a $(288, 495, 436, 8)$ tensor. The first two of the 8 channels encode the aggregated volume and average speed of all underlying probes whose heading is between 0 and 90 degrees (*i. e.* NE), the next two the same aggregation of volume and speed for all probes heading SE, the following two for SW and NW, respectively. The test set for each city in both competitions asked to make 100 predictions spread over 180 days of the dynamic probe data portion, each predicting 8-channels and 6 time slots (5, 10, 15, 30, 45 and 60 minutes into the future). Each single test set thus contains a $(12, 495, 436, 8)$ tensor and participants are required to return a prediction consisting of a $(6, 495, 436, 8)$ tensor for this test set. In addition, for each test, a (2) tensor is provided: the first channel indicates the day of week (0 = Monday, ..., 6 = Sunday) and the second channel the time of day of the test slot (0, ..., 240) in local time.

All tensors are `uint8`.

With the focus of our proposed prediction tasks on the temporal and spatial transfer the data provided focuses on the dynamic channels from GPS data as well as the static channels encoding the properties and descriptive features of the road graph.

F.1.4. TEST DATA

For the temporal (core) challenge, tests were sampled uniformly in the target period (April/May 2020). For the spatio-temporal (extended) challenge, tests were sampled uniformly from April/May both 2019 and 2020. See the scatter plot of Figure 42. The year of the test slot was not revealed to participants, only time of day and day of week, see Section F.1.3.

Figure 43 shows the day of week distribution of the test slots, which are uniform for the core and extended challenges. Figure 44 again shows uniform sampling for the core and extended challenges.

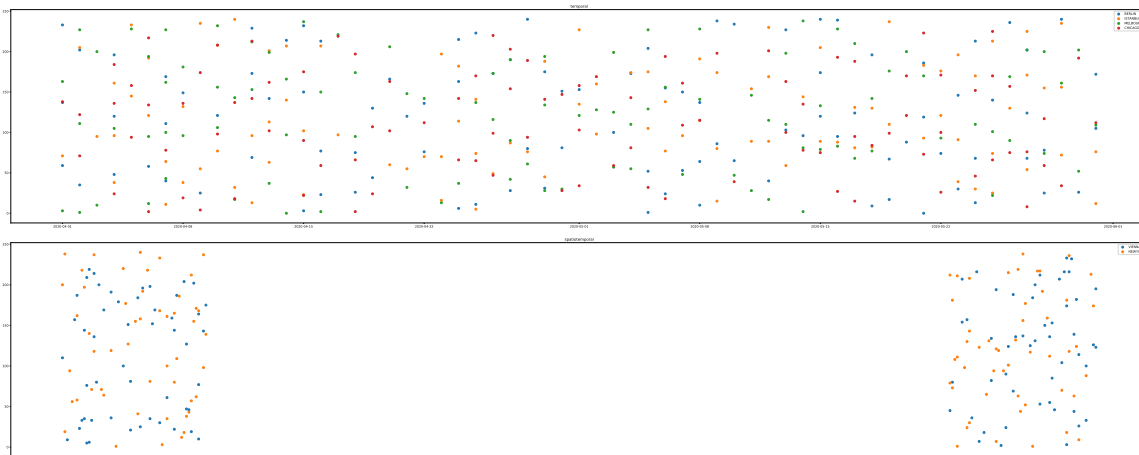


Figure 42: Distribution of first slot of test input for temporal (top) and spatio-temporal challenge (bottom). The 100 slots per city for the temporal (core) challenge are sampled uniformly from April and May 2020, the 100 slots per city for the (extended) spatio-temporal challenge are sampled uniformly from April and May both 2019 and 2020. Test slots start at time 0,...,240 (8PM local time).

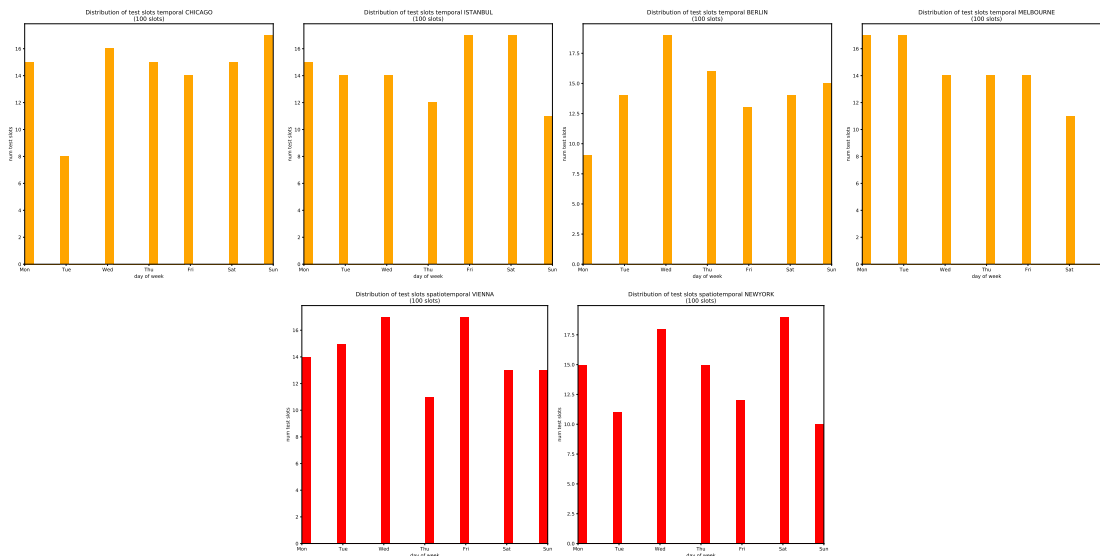


Figure 43: Per-city day of week distribution of test slots for temporal (core, yellow) and spatio-temporal (extended, red) competitions.

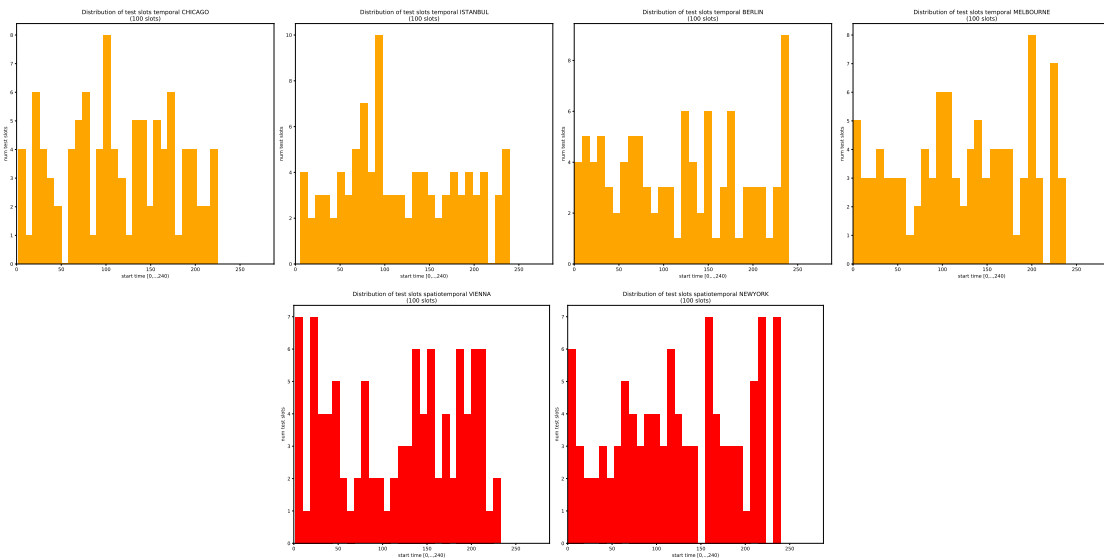


Figure 44: Per-city time of day distribution of test slots starting times for temporal (core, yellow) and spatio-temporal (extended, red) competitions.

F.2. Temporal Shift from pre-COVID to in-COVID

This section gives an illustration of the temporal shift in the data which gave rise to the design of the core competition as a temporal domain-transfer task (see Section E.2). In the plots below (Figures 45–48), we compare volumes for some example cities in the competition for the pre-Covid (April/May 2019) and the in-Covid (April/May 2020) regimes, respectively.

The plots show the sum of the volume for all four heading directions over all 288 5-minute bins of the day. We see a clear shift in the relative volumes for all cities. Note, volumes in each pixel are capped and normalized during the data preparation and, hence, the sums are not reflecting the absolute volume and, therefore, we do not label the y-axis in the plots below. Also, we normalized all data-sets to local time instead of UTC to have comparable curves.

Looking at Istanbul (Fig. 45), we can see a clear reduction in volume while the general pattern of traffic volume evolution during the day remains quite similar. The curfews in Turkey in 2020 were only limited to certain age groups and weekends.

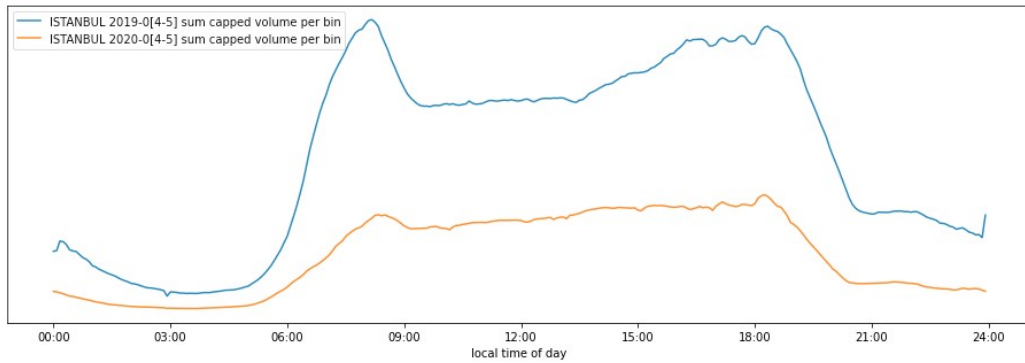


Figure 45: Istanbul traffic volumes per time of day pre-COVID vs in-COVID

The plot of Berlin (Fig. 46) shows that the measures in Germany seem to have dampened the morning commute quite considerably while the afternoon peak still got to almost pre-pandemic level.

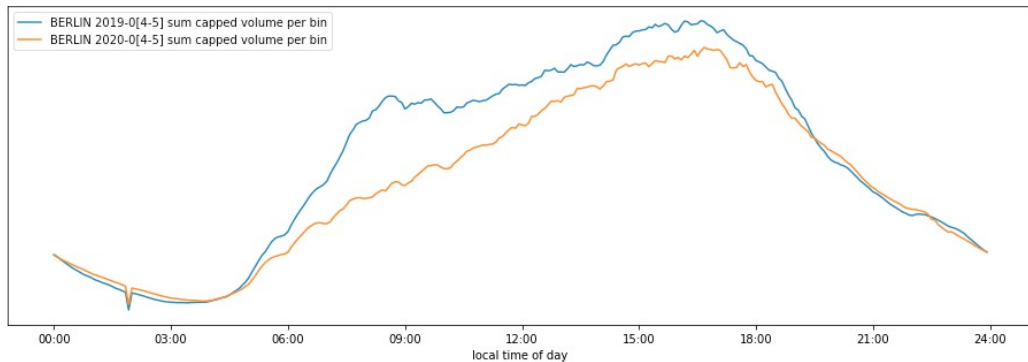


Figure 46: Berlin traffic volumes per time of day pre-COVID vs in-COVID

In contrast, in Barcelona (Fig. 47), it seems that the strict curfew in Spain had a clear effect on mobility during evening hours while the pattern of regular day mobility remained similar at reduced volume.

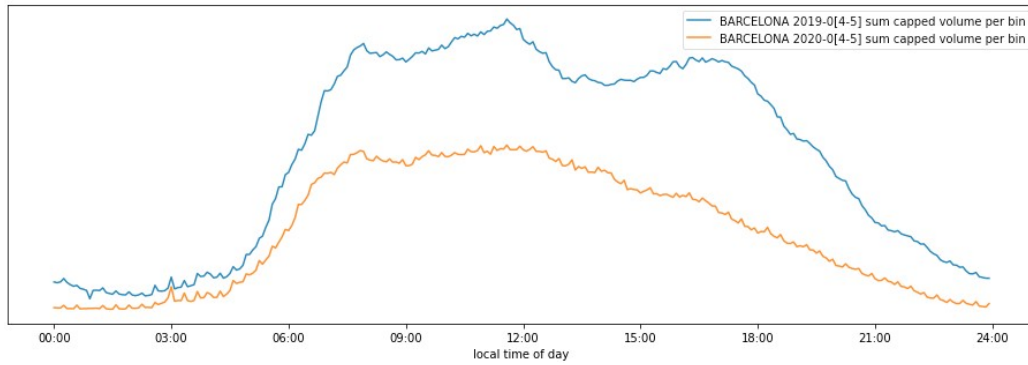


Figure 47: Barcelona traffic volumes per time of day pre-COVID vs in-COVID

Finally, in New York (Fig. 48), we see that the general pattern of traffic volumes was also preserved during April and May 2020, however at a significantly reduced volume.

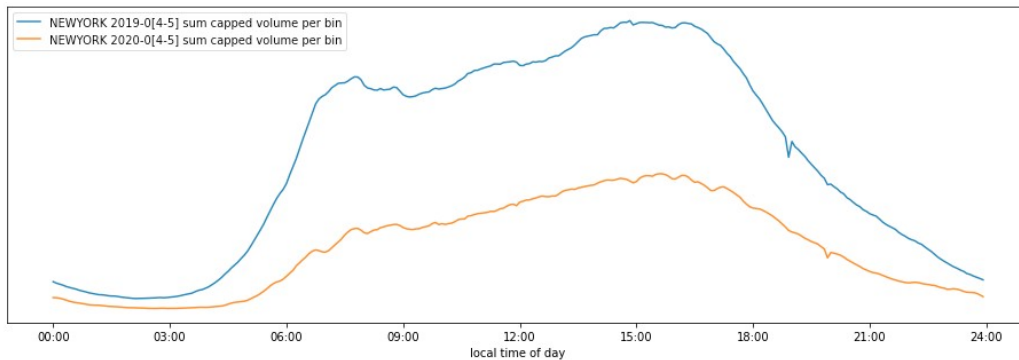


Figure 48: New York traffic volumes per time of day pre-COVID vs in-COVID

F.3. Exploring the Spatial Data Properties

This section provides additional information on the inherent temporal and spatial sparsity properties of the provided in different cities and in different regions of the same city. The provided examples show how the differences in coverage as well as in update frequency of different pixels are visible in the data.

F.3.1. CITY-SPECIFIC BIASES

From the simple rendering of the road network in Figure 49 already a quite significant difference in the density of the road network is visible. This is, of course, also related to the population density (Berlin 3.8M, Istanbul 15.5M, Moscow 12.9M, Chicago 2.9M) and other socio-economic parameters such as housing types. In addition to the available

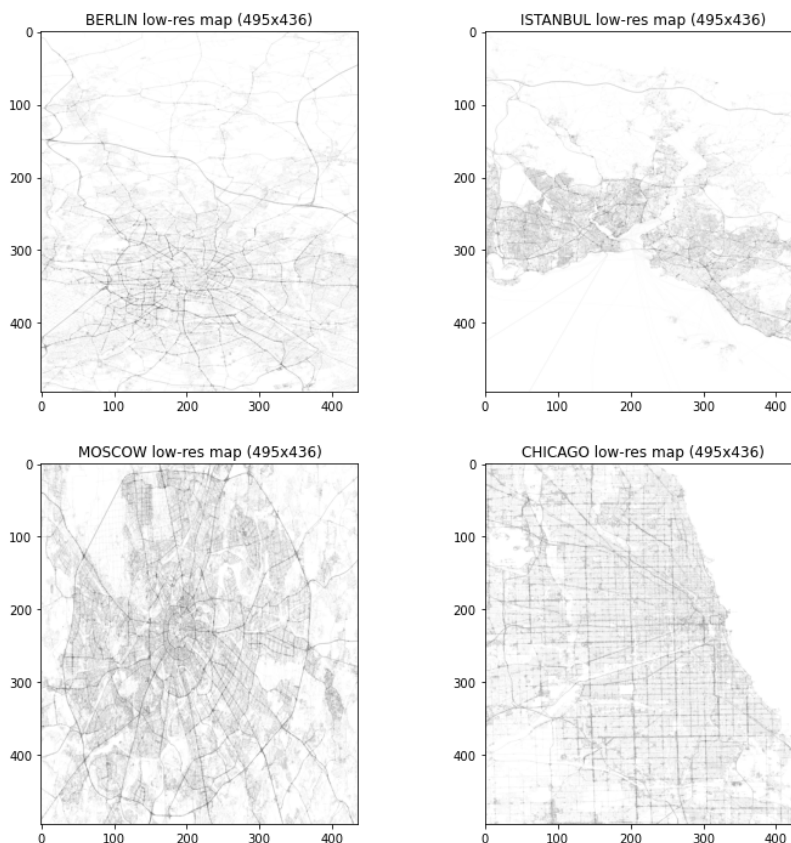


Figure 49: Simple rendering of the low-res road map in 4 competition cities

road network, there are also other parameters and biases in the GPS data which was used to generate the competition probe data movies. The GPS recordings represent only a sub-sample of the total traffic in a city and they can have different frequencies and other temporal patterns dependent on the city and on the fleets which contributed their data. In addition to this “city bias”, there are also differences in the frequency and stability of the recordings dependent on the area of the city. This “collection bias” is not systematic and

can only be assessed empirically. Information on the fleets and recording details are not shared by the data provider.

F.3.2. VOLUME AND SPEED – COVERAGE AND FREQUENCY

In order to illustrate the variance in terms of coverage and frequency in the data, we picked three example areas in Berlin (see Fig. 50). #1 is a highway in the outskirts and #2 a highway at the main ring-road. #3 shows a boulevard in the center of Berlin with business as well as housing.

The general distributions of volumes and speeds in these areas is shown in Figure 50. The volumes display the differences between a less frequently visited outskirts areas (#1) and city center areas (#2 and #3). Regarding speeds, the highway in #1 has higher speeds reported due to a higher speed limit and less traffic. The highway in #2 has a lower speed limit and more traffic causing lower speeds during the day (see also below). The boulevard (#3) has low speeds as expected.

F.3.3. VOLUME AND SPEED – EVOLUTION THROUGHOUT A DAY

For further analysis we pick a single cell (see Fig. 50 and 51) at the center of the areas from Figure 50 for having a look at the volume and speed throughout an example day.

Figure 52 shows the speeds as red lines and the volumes as blue bars for the selected pixels on a Wednesday in 2019. If no volume is reported (volume 0 or below privacy threshold), the speed is also 0. In the first plot for area #1 we see the normal daily pattern with increasing volume during morning and evening rush hour but no congestion as we are in the outskirts. In the second plot for area #2, we see the volume evolution during the day with the speeds indicating congestion and lower speeds during the day especially during morning and afternoon hours with a congestion between 6pm and 7pm. The third plot for area #3 shows the city boulevard with very flaky data as speeds are generally low and volumes are spiky with *e. g.* cars stopping.

In contrast, Figure 53 show speeds and volumes for the same pixels, however for a Sunday in 2019. The reduced volume in early morning hours are clearly visible in all three plots, while the second plot for area #2 also reports heavy traffic on the ring road in the late morning.

F.3.4. WHY DOES THIS MATTER?

The examples shown in this section explore the sparsity of the input data. Both in terms of volume and speed the coverage as well as the update frequency do differ within a city and between cities. In order to properly predict the traffic volume, models need to be able to cope with this sparsity.

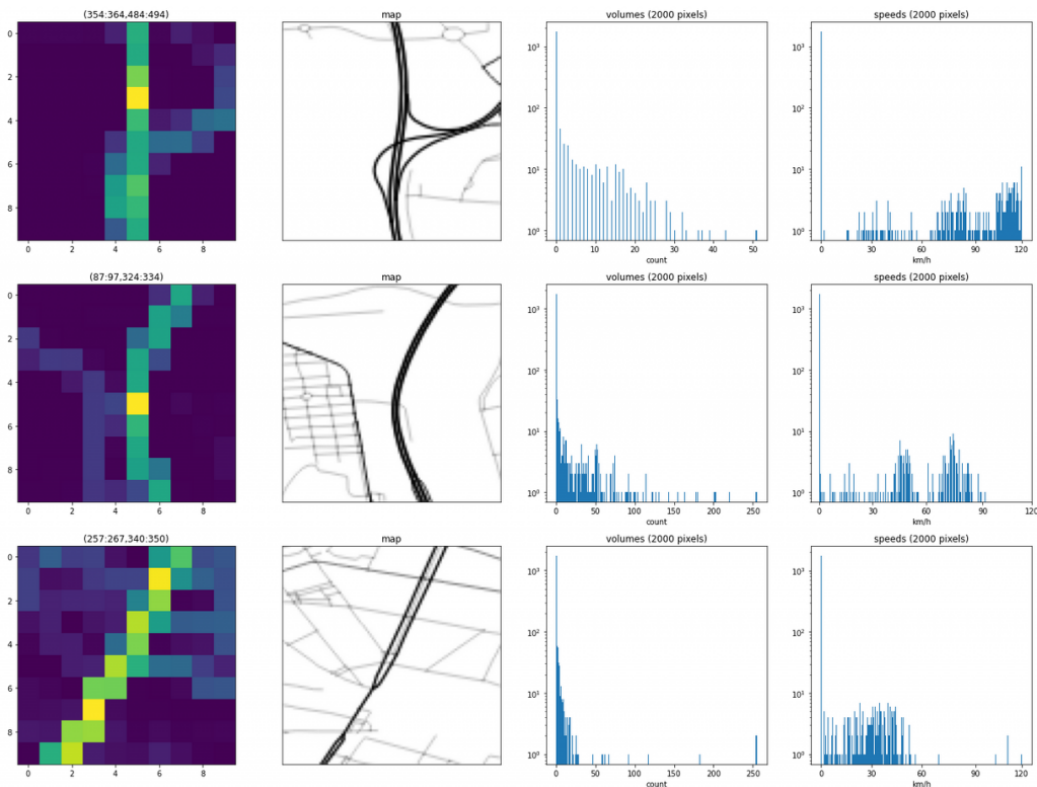


Figure 50: Three example areas in Berlin with volume heat map, road map, volume and speed histograms. The second column shows the map for illustration purposes. The third and fourth columns show histograms of the recorded normalized volumes (4 channels) as well as the speeds (4 channels) during a 5 minute slot at 10am (collected for 5 consecutive days for better visibility) from a 10×10 area. The first column shows a log sum heatmap over all channels of the pixels in the selected area for the same data.

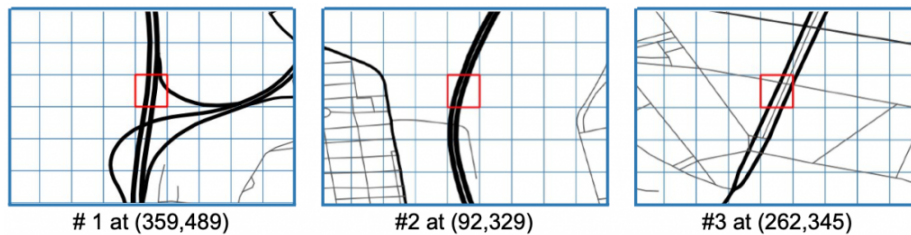


Figure 51: Three example areas in Berlin with chosen pixels (red box) for further analysis of NE heading.

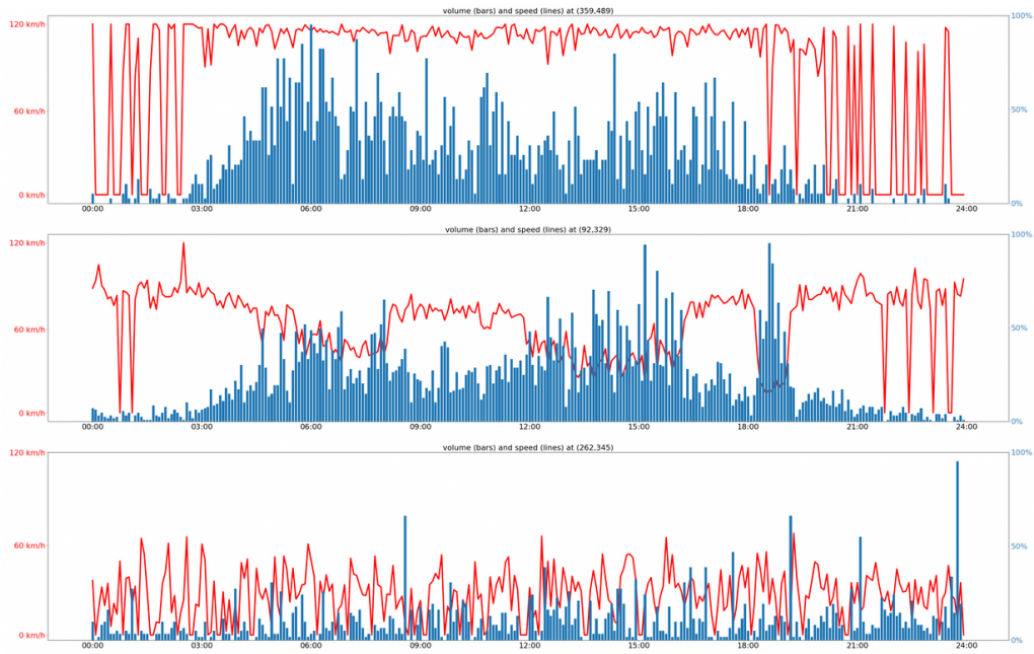


Figure 52: Volume (blue bars) and speed patterns (red line) for the selected pixels in NE heading on a Wednesday in 2019

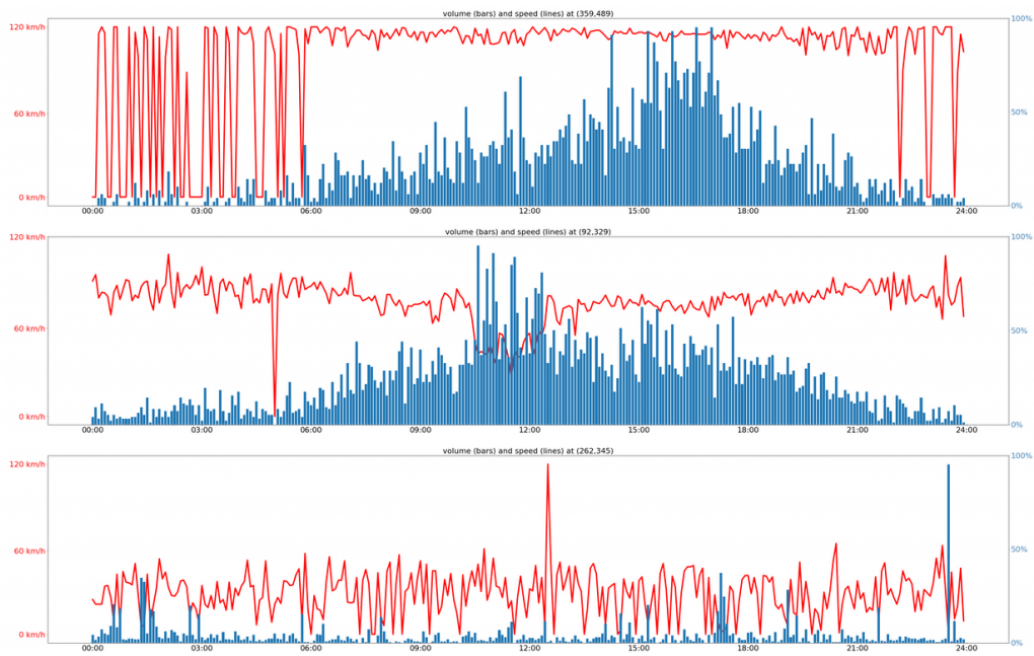


Figure 53: Volume and speed patterns for the selected pixels on a Sunday in 2019

Appendix G. MSE Details

G.1. Spatially Masked MSE

This section has a look at differences between a full and a masked MSE. In particular it is important to see whether the image-focused MSE also works for the traffic map prediction where *e.g.* graph-based approaches would only predict in areas covered by the road graph.

For the illustration we are using a prediction for Istanbul using the naive average baseline¹, which takes the average over all input data for all 6 predictions. Istanbul is a “hard” example since, due to the waterways in the city, there are more non-road areas with traffic than in other cities. On the waterways vehicles are not following exactly the same path and hence a road-mask would not work, these variances are visible in the movie visualizations of the data.

The value distribution in Figure 54 (bottom right) shows that the small number of affected pixels is quite homogeneously distributed. And, in the specific example of Istanbul, the difference of the masked MSE vs the normal one is approx. 0.4. Table 4 shows the “graph only” difference for all cities in the core challenge and as expected, Istanbul is by far most affected and overall, the differences are even smaller.

city	full mse	both masked ^a	Δ both masked	graph only ^b	Δ graph only	test slots
Istanbul	68.041132	67.018380	1.022752	68.410726	-0.369594	50
Berlin	97.128263	96.426923	0.701340	97.270101	-0.141838	50
Melbourne	36.198404	36.133144	0.065290	36.195613	0.002791	50
Chicago	45.284226	45.246546	0.037681	45.282553	0.001673	50
All	61.663006	61.206241	0.456766	61.789748	-0.126742	200

Table 4: MSE “both masked” and “graph only” difference for all cities in the core challenge.

Data comes from 5 days of the training data and 10 time slots, predictions using the “naive average baseline” (taking the average of the input as output for all 6 time slots in the future for every pixel and channel). ^a mask applied to prediction and ground truth. ^b mask applied to prediction only.

The examples shown here can also be reproduced and explored in more detail in the notebook provided in the competition GitHub repo².

¹https://github.com/iarai/NeurIPS2021-traffic4cast/blob/master/baselines/naive_average.py

²<https://github.com/iarai/NeurIPS2021-traffic4cast/blob/master/metrics/metrics.ipynb>

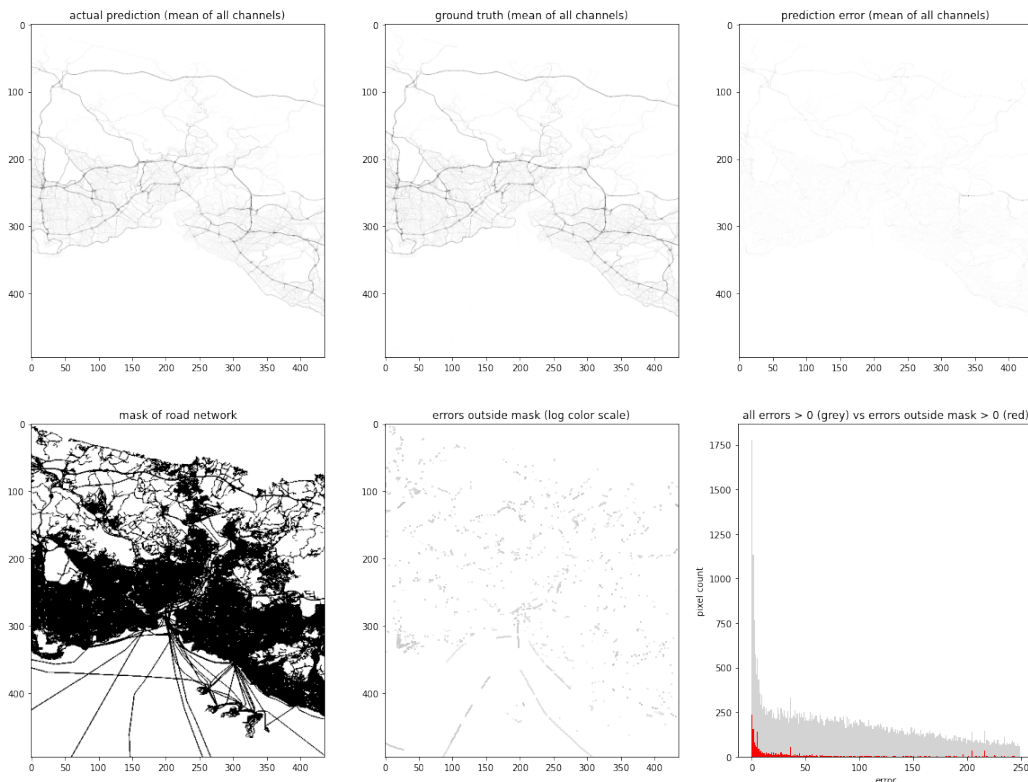


Figure 54: Illustrations of the masking in Istanbul. The first row shows the mean over all 8 channels for the actual prediction (left) and the ground truth (middle) for the full prediction horizon. The plot on the right-hand side shows the per-pixel mean squared prediction error (prediction – ground-truth) and one can already see that the visible errors are actually in areas where there are also important roads. The mask, shown in the bottom left plot, is based on the static road map which is provided as part of the competition data (1 for all pixels intersected by a road, 0 everywhere else). In the middle in the bottom row, only the prediction errors that would be masked away are shown. This output has been exaggerated logarithmically in order to visually see the small pixel errors from the ferry lines in the lower middle of the map. The bottom-right histogram shows the value distributions for the prediction error. The x-axis shows the magnitude of the error while the y-axis indicates the count of affected pixels. The red bars in the plot show the portion of the errors that the mask would take away.

G.2. Exploring MSE

This section uses the naive average baseline³ to explore how the MSE behaves and where models might struggle. Figure 55 shows the general MSE levels of the different channels for the example from Berlin. It is clearly visible that the general level of the MSE for speed values is significantly higher than the volume MSE.

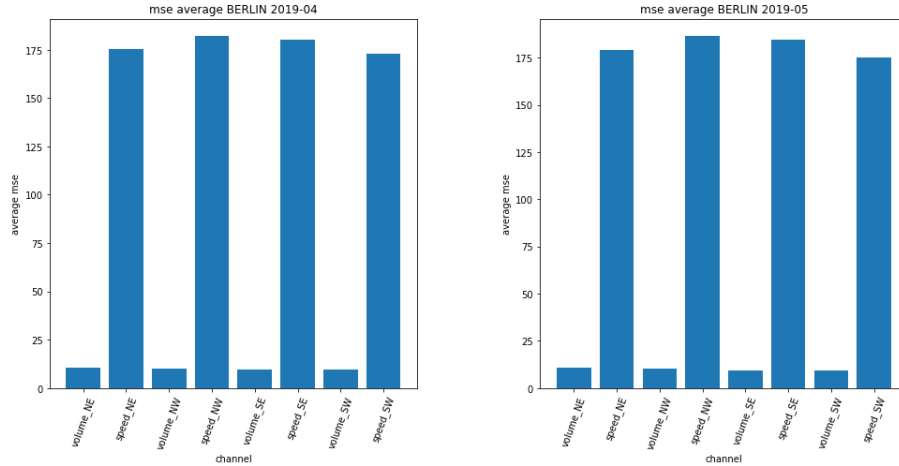


Figure 55: Naive average baseline MSE per channel (speed and volume in 4 heading directions). Data from 3 sample days in Berlin from April 2019 (left) and May 2019 (right), 22 tests per day starting at every full day.

The temporal dimension of the MSE is shown in Figure 56, we see that averaging over the input sequence follows the general peak pattern.

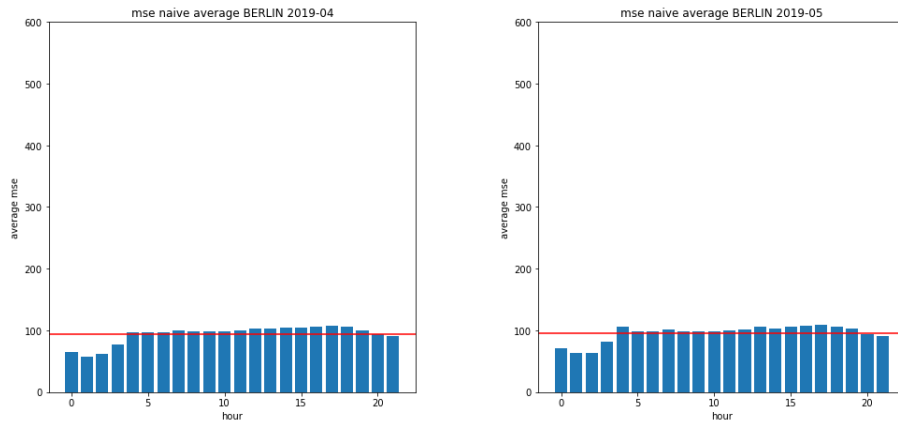


Figure 56: Naive average baseline MSE throughout the day (hourly averages). Same data as in Fig. 55.

³https://github.com/iarai/NeurIPS2021-traffic4cast/blob/master/baselines/naive_average.py

Figure 57 shows the quality of the prediction over the prediction horizon. As expected, naive averaging is better in the next slots to predict, but the ascent is not as steep as one might have expected.

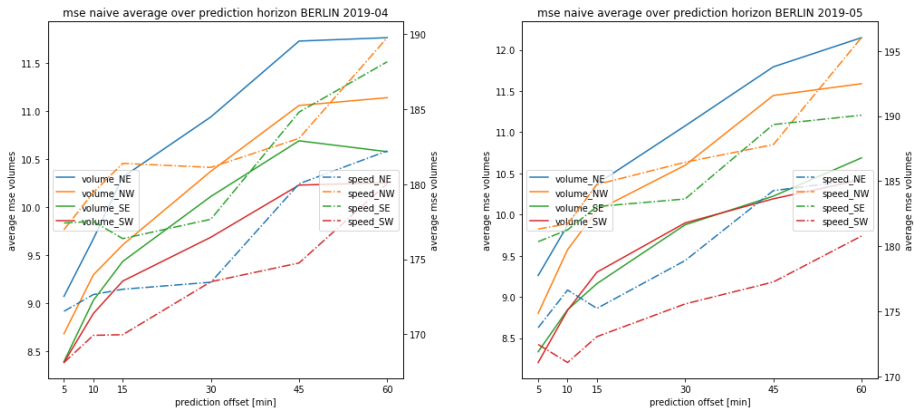


Figure 57: Naive average baseline MSE over the prediction horizon (5, 10, 15, 30, 45 and 60 minutes) and per channel. Notice the different scales for volume (left) and speed (right). Same data as in Fig. 55.

Per-pixel loss is largest on most used roads, both in volume and speed in the examples in Figure 58.

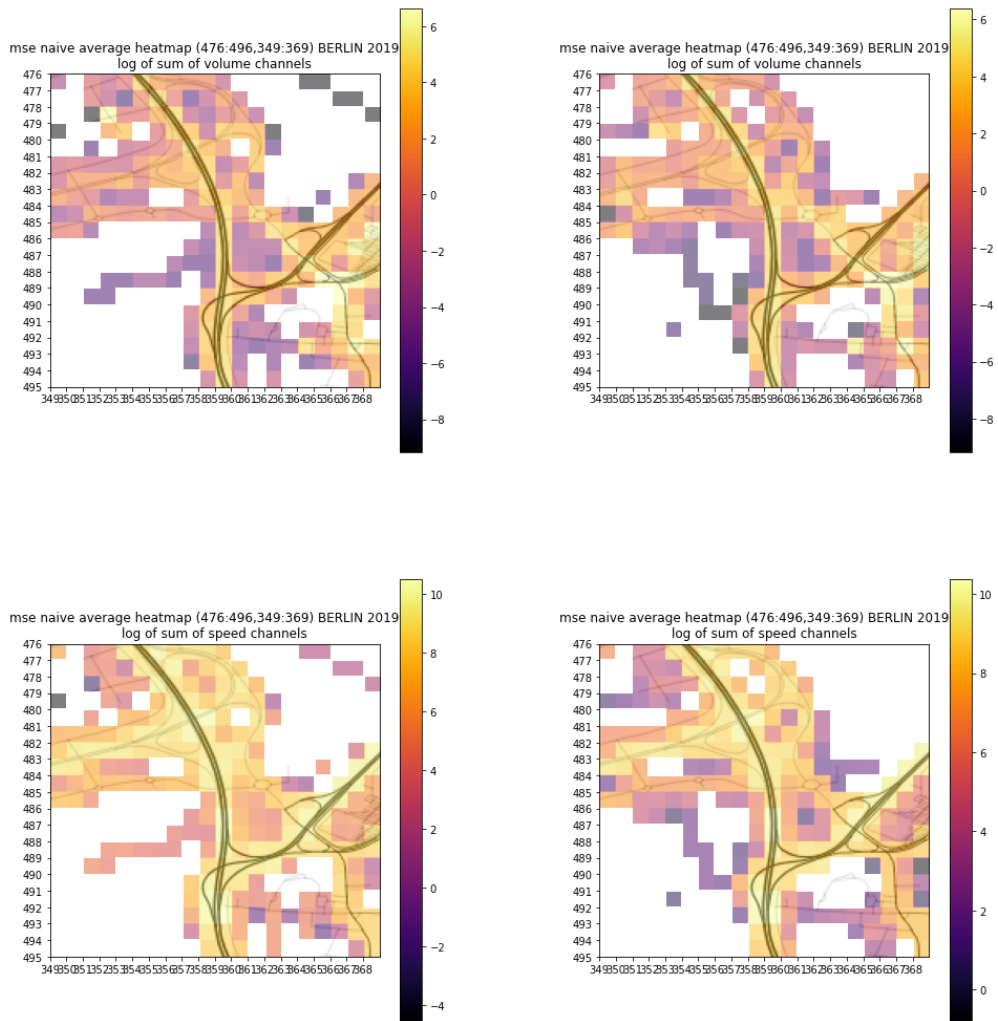


Figure 58: Naive average baseline MSE heatmap (per pixel, volume top row and speed bottom row) for a 10×10 area in Berlin. Same data as in Fig. 55.

Appendix H. Baselines

Here, we describe in more detail the two non-trivial baselines (see also Table 5) provided.

For the core competition, we used a vanilla U-Net (Ronneberger et al., 2015) and trained a separate model for each city for 4 epochs on the city’s 2019 training data⁴.

For the extended competition, a Graph ResNet was used following (Martin et al., 2020b). In contrast to them, we do not derive the graph from dynamic data, but derive it from the static data provided in the competition. We used a 194’000 training samples from BERLIN for one epoch. We enumerate the nodes of this graph; this enumeration corresponds to a subset of all the pixels (0,0),…,(494,435). This allows us to represent the graph’s edges as pairs of integers. In addition, we pass the dynamic data indexed by the enumerated nodes. The dynamic data not covered by the graph is discarded. This data object is then used to train a graph resnet. In summary, the input to the graph res net is a `torch_geometric` data object consisting of

```
x: (num_nodes, 12 * 8) float tensor
edge_index: (num_edges,2) long tensor
y: (num_nodes, 6*8) float tensor
```

This data object is then used to train a graph resnet. Here, the input of the current layer is added to the output of the current layer before passing it on to the next graph residual block as shown in Figure 59.

⁴The code for the U-Net baseline can be found at https://github.com/iarai/NeurIPS2021-traffic4cast/blob/master/baselines/baselines_unet_separate.py.

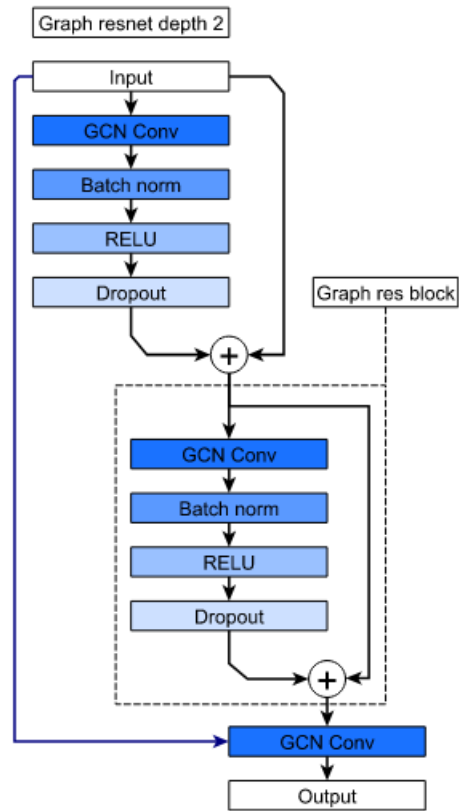


Figure 59: Graph res net architecture from (Martin et al., 2020b), reprinted with permission, based on (Kipf and Welling, 2017).

We deliberately did not explore fine-tuning and approaches feeding the output of the graph resnet to a U-net for instance. We did not want to bias participants too much in the hope our code can help participants get started more quickly⁵.

Table 5 gives an overview of the two baselines.

Team, rank (core/ext), approach	road graph, time-of-day, day-of-week ^a	models trained p. city ^b	#models trained ^c	Training datasets ^d	\sum #params core / ext ^e	mask ^f
moritzneun (11/-) separate U-Net	no	no	4 / -	{C[1-4]}/-	31.1M/-	-
christian (-/8) Graph ResNet	road graph	no	-/1	-/{C1}	-/0.2M	-

Table 5: Synopsis for our baselines. ^a what supplemental information is used; ^b whether some of the trained models used in the inference are specifically trained on the target city; ^c 9/7 means 9 models in the core and 7 different models in the extended competition, whereas 1=1 means the same trained model was used in both competition; ^d T1=Moscow, T2=Barcelona, T3=Antwerp, T4=Bangkok, C1=Berlin, C2=Istanbul, C3=Melbourne, C4=Chicago, E1=Vienna, E2=New York, T*=all training cities, C*=all core cities, E*=all extended cities, *e. g.* (9/7) \times {T*,C*} means 9 models trained on all training and core competition cities for the core competition and 7 from the same cities for the extended competition, and {T*,C[1-4]} expands to a model for each city trained on all training cities plus one of the core cities; ^e Sum of trainable weights of all the model checkpoints used in the inference; ^f Kind of mask used for post-processing..

⁵The code can be found under https://github.com/iarai/NeurIPS2021-traffic4cast/blob/master/baselines/graph_models.py. The call was: `python baselines/baselines_cli.py --model_str=gcn --limit=200000 --epochs=1 --batch_size=5 --num_workers=16 --train_fraction=0.97 --val_fraction=0.03 --file_filter="**/*BERLIN*8ch.h5"`.